AD-A150 435 THERMAL AND THERMOELASTIC EFFECTS IN ROLLING/SLIDING CONTACTS(U) NORTH CAROLINA STATE UNIV AT RALEIGH NC PRECISION ENGINEERING LAB T A DOW ET AL. 30 SEP 84 1/1

UNCLASSIFIED EEL-005 N00014-82-K-0551 F/G 20/13 NL

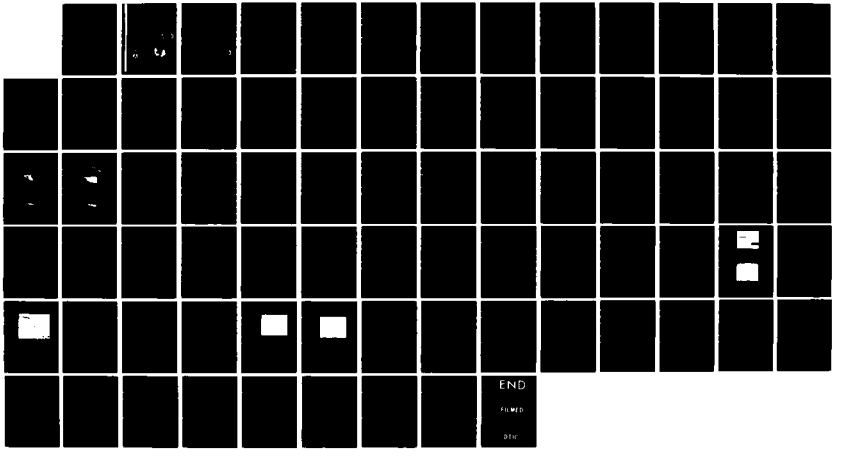

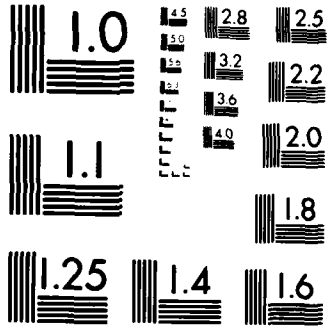

MICROCOPY RESOLUTION TEST CHART
NATIONAL BUREAU OF STANDARDS 1963-A

(6)

Final Report

on

Thermal and Thermoelastic Effects in Rolling/Sliding Contacts

North Carolina State University

Precision Engineering Laboratory

Final Report

on

Thermal and Thermoelastic Effects in Rolling/Sliding Contacts

to

Office of Naval Research

800 N. Quincy Street

Arlington, VA

Contract Number ONR - N00014-82-K-0551

June 1, 1982 - September 30, 1984

By

T. A. Dow

D. K. Lawson

F. Sadeghi

from

North Carolina State University

Raleigh, NC

SECURITY CLASSIFICATION OF THIS PAGE (When Data Entered)

REPORT DOCUMENTATION PAGE		READ INSTRUCTIONS BEFORE COMPLETING FORM
1. REPORT NUMBER	2. GOVT ACCESSION NO. AD-A165 435	3. RECIPIENT'S CATALOG NUMBER
4. TITLE (and Subtitle) Thermal and Thermoelastic Effects in Rolling/Sliding Contacts		5. TYPE OF REPORT & PERIOD COVERED Final June 1, 1982 - Sept. 30, 1984
		6. PERFORMING ORG. REPORT NUMBER PEL 005
7. AUTHOR(s) T. A. Dow D. K. Lawson F. Sadeghi		8. CONTRACT OR GRANT NUMBER(s) N00014-82-K-0551
9. PERFORMING ORGANIZATION NAME AND ADDRESS Precision Enigneering Laboratory, Box 7910 North Carolina State University Raleigh, NC 27695		10. PROGRAM ELEMENT, PROJECT, TASK AREA & WORK UNIT NUMBERS
11. CONTROLLING OFFICE NAME AND ADDRESS Georgia Institute of Technology 206 O'Keefe Building Atlanta, GA 30332		12. REPORT DATE June 1, 1982-Sept. 30, 1984
		13. NUMBER OF PAGES 74
14. MONITORING AGENCY NAME & ADDRESS(if different from Controlling Office) Office of Naval Research 800 N. Quincy St. Code 432 Arlington, VA 22217		15. SECURITY CLASS. (of this report) unclassified
		15a. DECLASSIFICATION/DOWNGRADING SCHEDULE

16. DISTRIBUTION STATEMENT (of this Report)

DISTRIBUTION STATEMENT A
Approved for public release
Distribution Unlimited

17. DISTRIBUTION STATEMENT (of the abstract entered in Block 20, if different from Report)

Approved for public release; distribution unlimited.

18. SUPPLEMENTARY NOTES

19. KEY WORDS (Continue on reverse side if necessary and identify by block number)

Tribology, Elastohydrodynamic Lubrication, electrical Brush, Wear, Thermal Effects, Thermomechanical Effects, Lubricant Rheology, High Current Density Monolithic Electrical Brushes.

20. ABSTRACT (Continue on reverse side if necessary and identify by block number)

This report describes a theoretical and experimental study of thermal and thermomechanical effects on frictionally and electrically heated rolling/sliding surfaces. A 2-D thermal analysis is used to predict the temperature distribution through the thickness of the lubricant film in an elastohydrodynamic (EHD) contact. The relative magnitude of shear and compressive heating as well as the losses due to conduction and convection are compared for pure rolling and slip conditions.

DD FORM 1 JAN 73 1473 EDITION OF 1 NOV 65 IS OBSOLETE
S/N 0102-LF-014-6601

SECURITY CLASSIFICATION OF THIS PAGE (When Data Entered)

TABLE OF CONTENTS

TABLE OF CONTENTS (Continued)

SUMMARY

The objective of this program has been to study the interaction of thermal and mechanical effects in tribological systems. Heat generated at a rolling or sliding interface can affect the contact geometry through thermal distortion of the mating surfaces. This heat can be generated due to friction contact, shear heating from a fluid film, or frictional and electrical heating at a current carrying interface. Thermomechanical effects have the potential for increasing the severity of the contact and may lead to "sparking" behavior for electrical brushes or "scuffing" failure for high-pressure rolling/sliding contacts.

This report described the results of a two-year program aimed at studing thermomechanical interactions in high-pressure elastohydrodynamic rolling/sliding contacts, and high-current-density monolithic electrical brushes.

For EHD contacts, a thermal analysis throughout the fluid film is derived using experimental values for the pressure and temperature boundary conditions. The results indicate the magnitude of the fluid temperature distribution, the heat generated by shear and compression, as well as the heat lost due to conduction and convection. For the pure rolling case, the mid-film fluid temperature rises 3 times more than the wall temperature rise. The peak temperature coincides with the peak shear heating which occurs in the inlet zone at the maximum pressure gradient. For the slip case, the mid-film temperature rise is 6 times greater than the surface and the peak is moved toward the exit due to shear heating in the contact zone.

This analysis allows one to predict the heat generation in an EHD contact and the flow of that heat into the mating surfaces. This

analysis will be used in the future to predict the distortion of the surfaces.

The second part of the report deals with the contact of an electrical brush and slip-ring. The heat generation in this case is assumed to be primarily due to construction resistance at the actual contact areas. A series of experiments has been performed to study the nature of the contact is a function of current density and to see if a thermomechanical criteria can be used to predict brush wear. The report presents a wear model based on contact concentration from thermal expansion which shows excellent agreement with the experimental values for a range of brush materials.

INTRODUCTION

The science of Tribology (friction, lubrication, and wear) is basically the study of rolling/sliding interfaces. These are the crucial elements of bearings, gears, seals, and slip rings. The interface supports the load while allowing the relative motion inherent in the mechanism to take place.

The study of interfaces is as old as Tribology (which Dowson [1] dates to the early Egyptians), but serious analysis began with Reynolds and Summerfeld about 100 years ago. Much of the early work dealt with the lubricant flow through the bearing geometry and the resulting pressure distribution. These analysis were used to predict bearing performance for a given loading and assumed rigid bearing geometry. It became clear from Martin's analysis [2] in 1916 that such assumptions do not predict the performance observed for high pressure contacts like rolling-element bearings. Grubin [3] showed that the elastic deformation of the mating surfaces significantly influenced the fluid flow and, by including these effects he improved the predictive capability of the analysis.

Thus, the analysis of a rolling/sliding lubricated contact became one of simultaneously solving the fluid flow and elasticity equations to determine the film thickness for an applied load. Of crucial importance was the fluid model; that is, the relationship between the fluid viscosity and the pressure. In general such analysis overlooked the effect of temperature on the process. For pure rolling contact, the lubrication was considered to be isothermal; that is, the lubricant temperature was assumed constant. Some analyses [4] have provided methods for calculating the influence of thermal effects on the process, but in general these have failed to provide a complete picture of the thermal field.

In addition to the direct influence of temperature on fluid properties, there is a second important effect of temperature; that is, the change in shape of the body due to thermal expansion. The concept of thermomechanical interactions and their effect on the life of mechanisms has been extensively studied and three ONR sponsored conferences [5] have been organized. This concept states that conditions exist where the interaction between surface heating and surface shape change is instable; that is, an increase in heating leads to a change in surface shape which exacerbates the heating. Such unstable conditions have been shown to exist in systems ranging from lubricated face seals to electrical slip rings. The analysis of these unstable systems have been carried out for surfaces heated by a friction coefficient. Work is needed to study these systems heated by fluid shear to see if similiar effects can be predicted.

The research reported here is aimed at studying the influence of thermal effects on rolling and sliding interfaces. An analysis of the generation of heat at the interface of an EHD contact was performed as well as a study of thermoelastic effects which occur in an unlubricated electrically-heated slip ring. These two problems are part of a continuing study of thermal effects in Tribology at NC State. The goal of this research is to develop and test calculation procedures to predict thermal effects so that new mechanisms can be designed with a better understanding of operating conditions and life.

BACKGROUND

Thermal effects can have two distinct influences on Tribology related processes: first, they will influence the temperature field as the surfaces roll or slide on each other. Second, the temperatures can have a

feedback effect on the process through thermal expansion or distortion of the mating surfaces. A thorough understanding of the direct influence of temperature is necessary before the more complicated stability analysis, implied by the feedback effect, can be attempted.

Table 1 shows an overall plan for the study of thermal effects. It is divided into three tasks; the first two deal with EHD contacts and the third to unlubricated, electrically-heated contacts. These types of processes may be greatly influenced by thermal and thermoelastic effects. The goal is to develop an understanding of these processes which can be used to estimate contact temperatures and their effect on the friction or wear of the system. For the case of the EHD contacts, the bulk of the effort was expended on Task I which defines the heat input to the stability analysis of Task II. Task III did not require the complications of fluid flow calculations to produce an estimate of heat generation. For this task a simple analysis, plus experimental data, were used to predict the wear of electrographic brushes at high current densities. The background leading to the results published here is discussed next.

Thermal EHD Model

Thermal effects can play an important role in the performance of an EHD contact. The fluid in such contacts can separate the surfaces at extremely high contact pressures because the viscosity rises exponentially with pressure. However, temperature has a moderating effect on the viscosity and a $10^{o}C$ rise in temperature can offset the viscosity change due to a pressure increase of 28MPa (4000 psi). As a result, the analysis of the performance of an EHD contact could be greatly improved if thermal effects were taken into account.

TABLE 1. THERMAL AND THERMOELASTIC EFFECTS IN ROLLING/SLIDING CONTACTS

NORTH CAROLINA STATE UNIVERSITY
T. A. DOW, PRINCIPAL INVESTIGATOR

6-1-82 TO 9-30-84

TASK I-THERMAL EFFECTS IN ELASTOHYDRODYNAMIC (EDH) CONTACTS	TASK II-THERMOELASTIC EFFECTS IN EHD CONTACTS	TASK III- THERMOELASTIC EFFECTS IN SEALS AND ELECTRICAL BRUSHES
PROBLEM - TRACTION AND FILM THICKNESS IN BEARING CONTACTS DEPEND UPON LUBRICANT TEMPERATURE AND ITS INFLUENCE ON VISCOSITY.	PROBLEM - SCUFFING FAILURE OCCURS IN LOCALIZED REGION OF ROLLING/SLIDING CONTACTS IN GEARS, SEALS, ETC.	PROBLEM - TEMPERATURES GENERATED BY FRICTIONAL AND ELECTRICAL HEATING PRODUCE NON-UNIFORM THERMAL EXPANSION LEADING TO UNEVEN CONTACT AND HIGH WEAR.
SOLUTION - DERIVE THERMAL MODEL OF EHD CONTACT FROM EXPERIMENTALLY MEASURED TEMPERATURE AND PRESSURE DISTRIBUTIONS FOR DIFFERENT LUBRICANTS.	SOLUTION - STUDY THE INFLUENCE OF TEMPERATURES GENERATED IN ROLLING/SLIDING SYSTEMS ON CONTACT GEOMETRY.	SOLUTION - EXPERIMENTALLY AND ANALYTICALLY STUDY THE CONTACT OF SLIDING SURFACES AND DEFINE THE EFFECT OF THERMAL EXPANSION AND WEAR ON CONTACT.
RESULT - GENERAL MODEL FOR PREDICTION OF THERMAL EFFECTS IN EHD CONTACT FOR DIFFERENT LUBRICANT CHEMISTRIES.	RESULT - MODEL OF OPERATING CONDITIONS AND MATERIAL CONSTANTS WHICH PRODUCE SCUFFING FAILURE.	RESULT - MODEL OF SLIDING CONTACT PREDICTING THE OCCURANCE OF HOT SPOTS.

One problem with predicting temperatures is that, in the past, there were few experimental measurements available to check the results. This was changed by the development of thin film pressure and temperature transducers. These allowed not only a direct measurement of the surface temperature for realistic contact loads and geometries, but the important ability to compare the location of that temperature to the pressure distribution.

Before such experiments were made it was assumed that nearly isothermal conditions existed for pure rolling contacts and heating was mainly due to slip between the surfaces. As a result of a recent program for ONR, Kannel and Dow [6] have published data showing significant temperature rise for pure rolling conditions and even higher temperatures for rolling/sliding conditions. For example, the surface of a disk lubricated with a so-called "traction fluid" operating at 13 percent slip will increase by about 150 ^{o}C through the EHD contact. Significant viscosity change will occur with this temperature rise and the formation of boundary films may be enhanced at these high pressures and temperatures. Therefore, the ability to predict the actual surface temperatures in a bearing or gear is an important facet of understanding and designing these mechanisms.

Three-dimensional data for surface pressure and temperature throughout an EHD contact are available for three different lubricants, a range of peak pressures, and different roll/slide ratios. This data is being used to validate the theoretical model. The model is based on one published by Dow [7], which shows the magnitude of the sources of heat generation and the main dissipation modes which occur through the contact. This earlier model utilized the limited data presented in reference [6], but the more extensive data now available allow the model to be verified over a wide range of lubricant chemistries and operating conditions. The current

analysis uses a Newtonian model of fluid behavior but this may not be appropriate for all the lubricants studied.

The previous published work [6] was at relatively low pressures (700 Pa (100,000 psi) and less) and the minimum film thickness values were extrapolated from earlier X-ray measurements. The recent experiments have produced measurements of the pressure distribution, temperature distribution, traction force, and film thickness for maximum Hertz stresses up to 1700 MPa (250,000 psi) and slip up to about 5 percent. Data are available for the following oils:

(1) Synthetic paraffinic (XRM-109F)

(2) Polyphenyl ether (5P4E)

(3) Traction fluid (Santotrac 50).

This data should provide enough information to validate the theoretical model of heat generation in the contact. The next step will be to use this information in a feedback analysis to find unstable operating conditions. This latter task is planned for the coming year of the program.

Electrical Slip-rings

It is well established [8,9] that the real contact area between two bodies consists of several small discrete regions. For an electrical brush, these regions support the load as well as pass the current through a sliding interface. Therefore, these regions are heated by friction from the sliding of the slip-ring and by electrical resistance (constriction and contact) as the current passes through the brush. For the high current density experiments discussed here, the current passing through the brushes is assumed to produce nearly all of the heating and the contribution from friction is negligible.

Sparking at the brush/slip-ring interface has been observed [10,11] for high current density electrographitic brushes. The occurrence of sparking has been taken as a limit on the current capacity of the brush. The experiments and analysis described were designed to study the sparking phenomenon, define operating conditions and material parameters which influence its occurrence and, determine its effect on brush performance.

The analysis is based on a hypothesis which involves the influence of non-uniform temperature (and the resulting non-uniform expansion) on the size and location of the contact spots. This hypothesis continues the theme of this research program; that is, finding the influence of thermal effects on the performance of Tribological systems. For static contact of the brush and slip-ring without current flow, the distribution of the contacting regions should be randomly distributed over the brush face. The microscopic surface roughness of the two bodies and Hertzian deflections occurring at the interface produce these random contacts. However, once current is passed through the brush, the local thermal gradients due to electrical heating will produce non-uniform thermal

expansions near the contact regions and localize the contact. Thus, the brush contact will occur at one or more high temperature regions. The temperature-resistivity relationship for graphite [12] causes unstable heating of such contact points and can result in temperatures over 2000°C. Such high temperature contact regions appear as "hot spots" at the brush interface and are proposed as the source of the "sparking" behavior observed.

This report extends previous work [10,13,14] on this subject in which both frictional and electrical heating were addressed. These papers dealt with the role of heating, thermal expansion and wear on the contact of seals and brushes. The results discussed here show that the hypothesis described above leads to a model for brush wear that shows excellent agreement with measured values over a broad range of operating conditions and brush compositions.

DETAILS OF THE RESEARCH PROGRAM

Thermal EHD Analysis

Governing Equations

The analysis requires the iterative solution of the thermal Reynolds' equation, the two dimensional energy equation with the fluid properties functions of pressure and temperature, and the elasticity equation. In this section, the thermal Reynolds' equation, the energy equation, and the elasticity equation are developed. The set of equations developed are then solved numerically. The following assumptions were made in the development of the thermal Reynolds' equation, the energy equation, and the elasticity equation.

1) Pressure is constant across the film.
2) Inertia forces of the fluid are neglected.
3) The viscosity is only a function of pressure and temperature.
4) The film thickness throughout the contact zone is much smaller than the radii of the rollers so that the Reynolds' equation is valid.
5) Side leakage is neglected (2D flow field).
6) Thermal conductivity, specific heat, and thermal expansion do not vary with temperature or pressure.

Reynolds' Equation

The thermal Reynolds' equation can be derived from the equilibrium of an infinitesimal element shown in Figure 1.

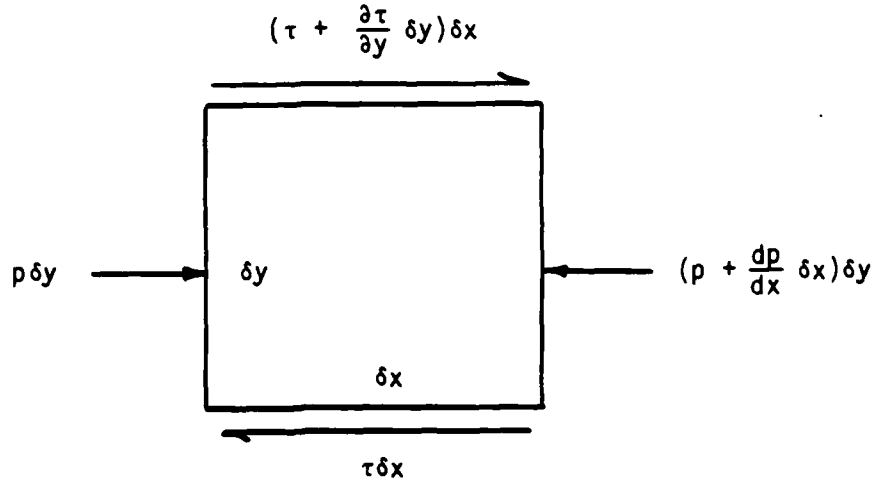

Figure 1. Forces Acting on a Fluid Element

Summing the forces in the x-direction (along the direction of flow) on the element we obtain;

$$P\delta y - (P + \frac{dp}{dx}\delta x)\delta y - \tau\delta x + (\tau + \frac{\delta \tau}{\delta y}\delta y)\delta x = 0$$

Therefore, equilibrium in the x-direction requires:

$$\frac{dp}{dx} = \frac{\partial \tau}{\partial y} \qquad (1)$$

A Newtonian fluid model is assumed with viscosity as a function of Pressure and Temperature, where $P = P(x)$, and $T = T(x,y)$. The shear stress is defined by

$$\tau = \mu \left(\frac{\partial u}{\partial y}\right)$$

Substituting τ in equation (1) we obtain;

$$\frac{dp}{dx} = \frac{\partial}{\partial y}\left(\mu\left(\frac{\partial u}{\partial Y}\right)\right)$$

From the above equation the velocity profile in the x-direction could be obtained:

$$u = \frac{dp}{dx}\int_0^y \frac{y}{\mu}\,dy + \left[\frac{u_2-u_1}{\mu_{e_0}} - \frac{\mu_{e_1}\frac{dp}{dx}}{\mu_{e_0}}\right]\int_0^y \frac{dy}{\mu} + u_1 \qquad (2)$$

where,

$$\mu_{e_0} = \int_0^h \frac{dy}{\mu}$$

$$\mu_{e_1} = \int_0^h \frac{y}{\mu}\,dy$$

From the velocity equation (2) and the flow equation given by

$$q_x = \int_0^h u\,dy, \qquad (3)$$

the thermal Reynolds' equation is obtained

$$\frac{\partial}{\partial x}\left(G_2\frac{dp}{dx}\right) = u_1\frac{\partial}{\partial x}(G_3) + \frac{\partial}{\partial x}\left[\frac{G_1}{\mu_{e_0}}(u_2 - u_1)\right] \qquad (4)$$

where,

$$G_1 = \int_0^h \left(\int_0^y \frac{dy}{\mu}\right) dy$$

$$G_2 = \frac{\mu_{e_1}}{\mu_{e_0}} G_1 - \int_0^h \left(\int_0^y \frac{y}{\mu}\,dy\right) dy$$

$$G_3 = \int_0^h dy$$

Film Shape

The film shape outside the high-pressure region is assumed to be the same as for Hertzian contact; that is,

$$h = \left(\frac{1-\nu_1^2}{E_1} + \frac{1-\nu_2^2}{E_2}\right) P_{max}\, a\left\{\frac{x}{a}\sqrt{\left(\frac{x^2}{a^2}-1\right)} - \ln\left[\frac{x}{a} + \sqrt{\left(\frac{x^2}{a^2}-1\right)}\right]\right\} \qquad (5)$$

The above equation is used to evaluate the film shape profile everywhere outside the contact zone, film thickness inside the contact zone is evaluated from the Reynolds' equation.

The Energy Equation

The temperature field within the lubricant film is obtained from the solution of the energy equation. Consider the elemental control volume shown in Figure 2 neglecting heat conduction in the direction of flow. The energy balance may be written as:

Energy convected in left face + energy convected in bottom face + heat conducted in bottom face + viscous work done on element + compression work done on element = energy convected out of right face + energy convected out of top face + energy conducted out of top face;

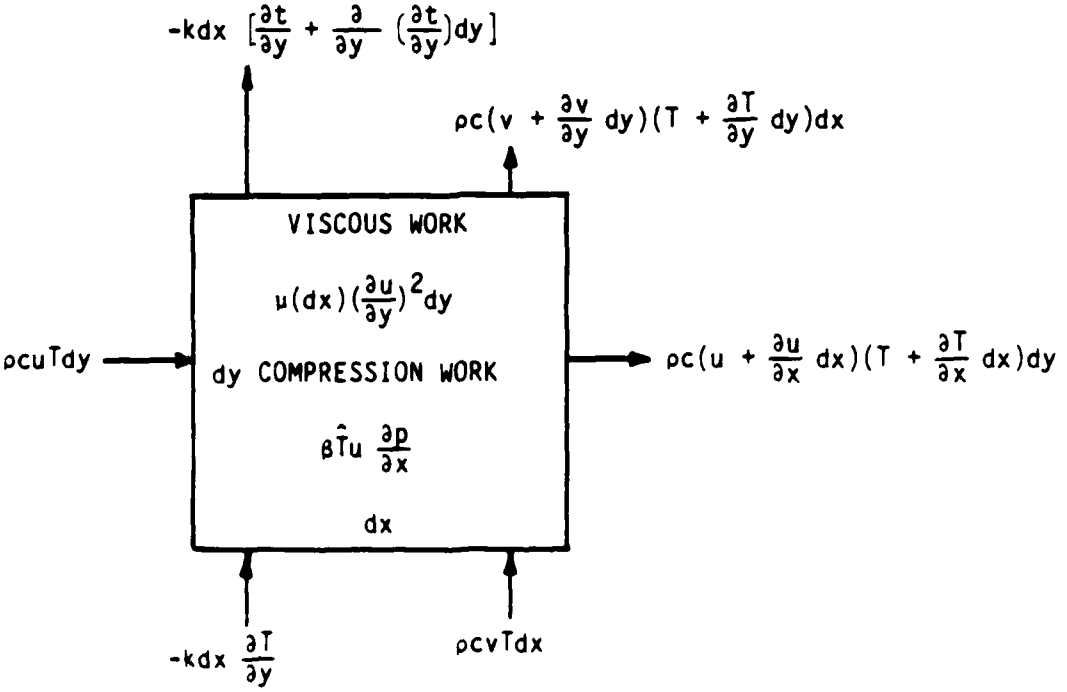

Figure 2. Energy Balance for a Fluid Element

Summing all the energies on the control volume produces:

$$\rho c(u \frac{\partial T}{\partial x} + V \frac{\partial T}{\partial y}) + T (\frac{\partial u}{\partial x} + \frac{\partial v}{\partial y}) = \mu(\frac{\partial u}{\partial y})^2 + \beta \hat{T} u \frac{\partial p}{\partial x} + K \frac{\partial^2 T}{\partial y^2} \qquad (6)$$

Continuity in the film requires that

$$\frac{\partial u}{\partial x} + \frac{\partial v}{\partial y} = 0 \qquad (7)$$

Substituting equation (7) into equation (6) the energy equation in a lubricated contact regime is obtained.

$$\rho c(u \frac{\partial T}{\partial x} + V \frac{\partial T}{\partial y}) = \mu(\frac{\partial u}{\partial y})^2 + \beta \hat{T} u \frac{\partial p}{\partial x} + K \frac{\partial^2 T}{\partial y^2} \qquad (8)$$

where

$$\frac{\partial u}{\partial y} = \frac{1}{\mu} [\frac{dp}{dx} (y - \frac{\mu_{e_1}}{\mu_{e_0}}) + \frac{u_2 - u_1}{\mu_{e_0}}]$$

Velocity Profiles in The Film

The velocity profile in the x-direction can be obtained from equilibrium of an infinitesimal element as shown in equation (2). The velocity profile in the y-direction can be obtained from the continuity equation:

$$\frac{\partial u}{\partial x} + \frac{\partial v}{\partial y} = 0$$

The continuity equation in this form is not well suited to evaluate v, since it is an initial-value problem needing only one boundary condition for its solution. If the continuity equation is differentiated with respect to y, it becomes:

$$\frac{\partial^2 v}{\partial y^2} = - \frac{\partial}{\partial y} (\frac{\partial u}{\partial x})$$

This equation is used to evaluate velocity in the y-direction using the finite difference method. Figure 3 illustrates variation of velocity in the rolling direction; backflow occurs in the film at the inlet zone and becomes a positive linear flow field at the center of the contact.

Rheological Fluid Model

The isothermal viscosity-pressure relationship used in this analysis was proposed by Roeland [15]:

$$\log \mu = (\log \mu_a + 1.2)\left(1 + \frac{P}{28400}\right)^Z - 1.2$$

An exponential change of viscosity with temperature was incorporated and the complete viscosity relationship can be expressed as

$$\mu = \frac{10^{\left[(\log\mu_a + 1.2)\left(1 + \frac{P}{28400}\right)^Z - 1.2\right]}}{e^{\delta(T - T_a)}}$$

Mass Flow Rate

The mass flow rate in an elastohydrodynamic lubrication contact with the temperature effects included can be written as:

$$q_x = u_1 G_3 - G_2 \frac{dp}{dx} + (u_2 - u_1)\frac{G_1}{\mu_{e0}}$$

Traction

The traction force (F_{shear}) is found by integrating the viscous shear forces on the disk surface, assuming a Newtonian fluid we obtain;

$$F \text{ shear} = F_1 - F_2$$

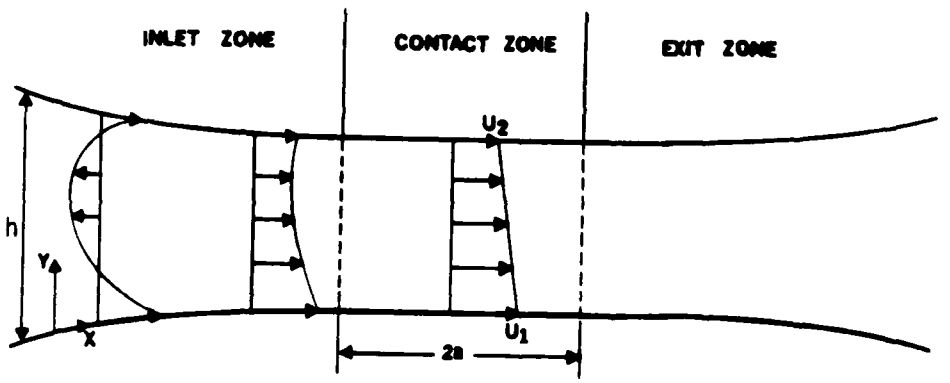

Figure 3. Velocity profile in a heavily loaded contact.

where

$$F_1 = \int_{-\infty}^{x_{exit}} \mu \left(\frac{\partial u}{\partial y}\right)_{y=0} dx$$

$$F_2 = \int_{-\infty}^{x_{exit}} \mu \left(\frac{\partial u}{\partial y}\right)_{y=h} dx$$

$$\frac{\partial u}{\partial y} = \frac{1}{\mu} \left[\frac{dp}{dx} \left(y - \frac{\mu_{e1}}{\mu_{e0}}\right) + \frac{u_2 - u_1}{\mu_{e0}} \right]$$

Computational Scheme

The solution to the thermal elastohydrodynamic problem utilizes an iterative approach starting with the flow field from the isothermal case. The isothermal solution is obtained with viscosity independent of temperature. The energy equation is then solved in finite difference form for the temperature distribution throughout the film. From this temperature distribution a new flow field is calculated and the process is repeated until the temperature distribution in the film converges to steady state. The convergence criteria is that each node of the temperature field from the current calculation must be within 0.1 percent of the previously calculated value.

One of the main problems in solving such fluid dynamics problems is evaluation of the substantial derivatives. These derivatives require a knowledge of the flow direction at each element before they can be evaluated. A formalized method of handling such problems is to utilize the "upwind" differencing scheme. The temperature at each surface is known from measured surface temperatures. It is also, assumed to be ambient at the entry nodes where the x-component of velocity, u, is positive. If the flow field predicts backflow at some entry nodes, the temperature at these nodes are dependent values and must be found during

the solution. The flow chart for the calculation procedure is shown in Figure 4.

One aspect of the solution technique which does not appear in the flow chart is the limitation on the temperature change per iteration. This procedure was designed to speed convergence and involves limiting the temperature change which can occur for a flow field change. The resulting temperature field is the same with or without using a limited temperature change, but convergence is reached considerably faster when the limiting temperature is used. Using the limitation that the temperature change will be less than or equal to 10% of the current temperature, the energy equation can be solved in 15-20 iterations.

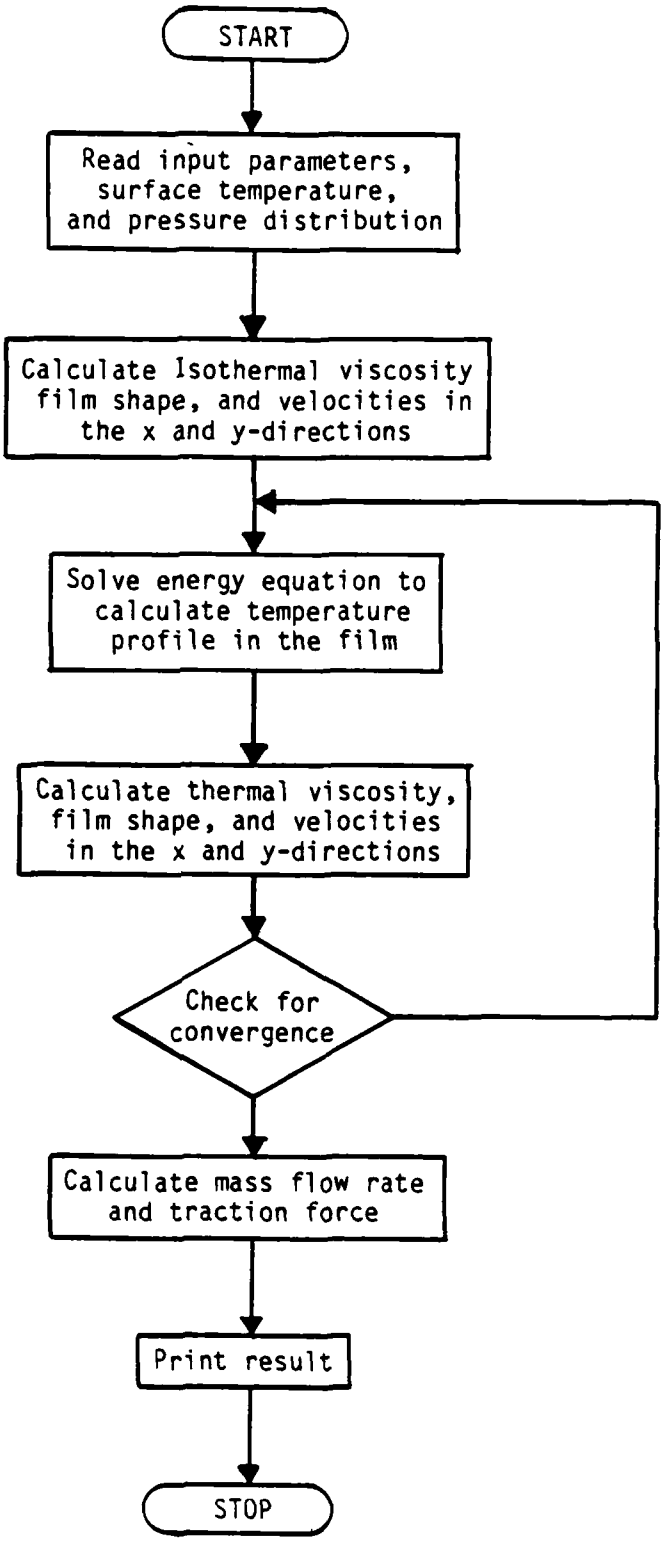

Figure 4. Flow Chart for Computational Scheme

Results and Discussion

Figures 5 and 6 present a three-dimensional picture of the pressure and temperature distribution in the conjunction region between disks for pure rolling and 6.2 percent slip respectively. These figures were assembled from a series of two-dimensional measurements (pressure vs. time and temperature vs. time) made at eight locations across the width of the contact. The peak pressure in each case is approximately 250,000 psi (1.72 GPa) and the lubricant was a synthetic paraffinic hydrocarbon (XRM-109).

These figures give an overall picture of the contact, but specific comparisons are more easily made using individual pressure and temperature traces. Figure 7 illustrates the pressure and temperature variation through the center of the contact for pure rolling and slip conditions. The pressure distribution, which is essentially the same in each case, orients the temperature distribution with respect to the contact. For the pure rolling case (Figure 7(a)), the peak surface temperature is 13°C above the ambient temperature; and the peak occurs in the inlet zone near the peak pressure gradient. For the 6.2 percent slip case (Figure 7(b)), the peak surface temperature is 25°C or a 90 percent increase from the pure rolling case. For slip conditions, the peak temperatue moves toward the center of the conjunction zone.

The two-dimensional analysis of the conjunction zone was used to predict the flow field and the resulting temperature distribution in the lubricant film. This analysis is applicable to the center of the contact where the pressure gradient in the width direction is zero. The data of Figure 7 was used as input data to the analysis and the materials and operating conditions are shown in in table 2. Measured data for traction and film thickness are presented in table 3.

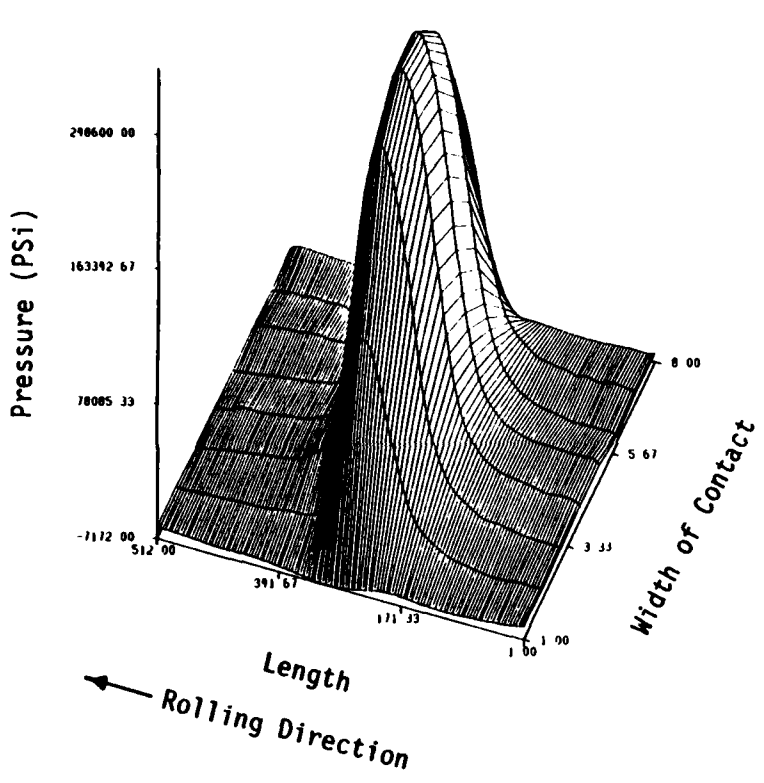

a) Pressure Distribution

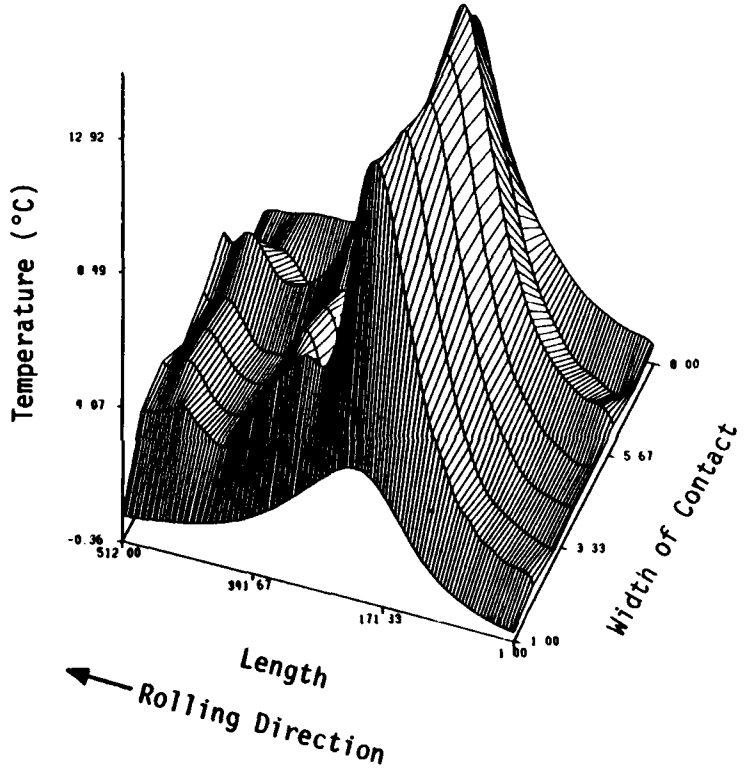

b) Temperature Distribution Above Ambient

Figure 5. Pressure and temperature distribuiton for pure rolling conditions.

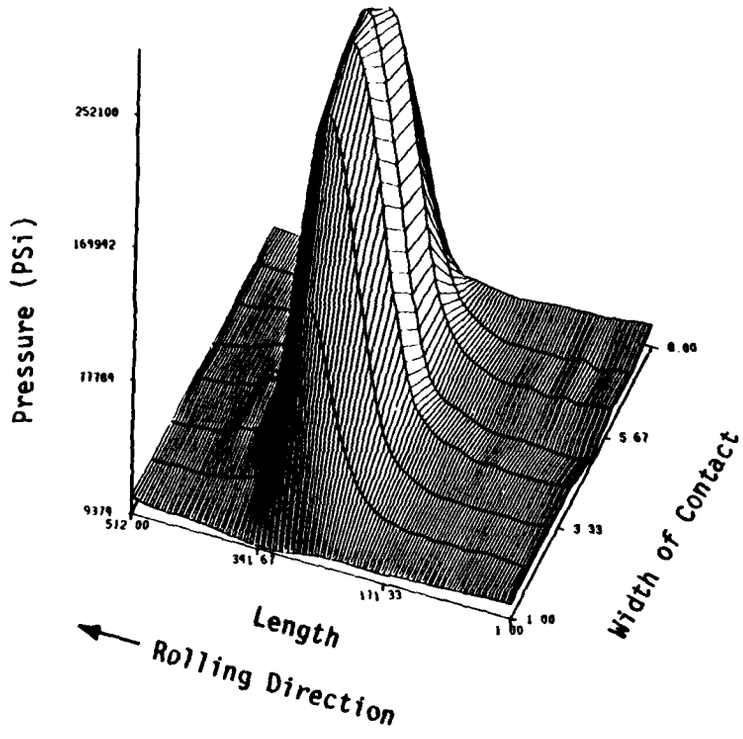

a) Pressure Distribution

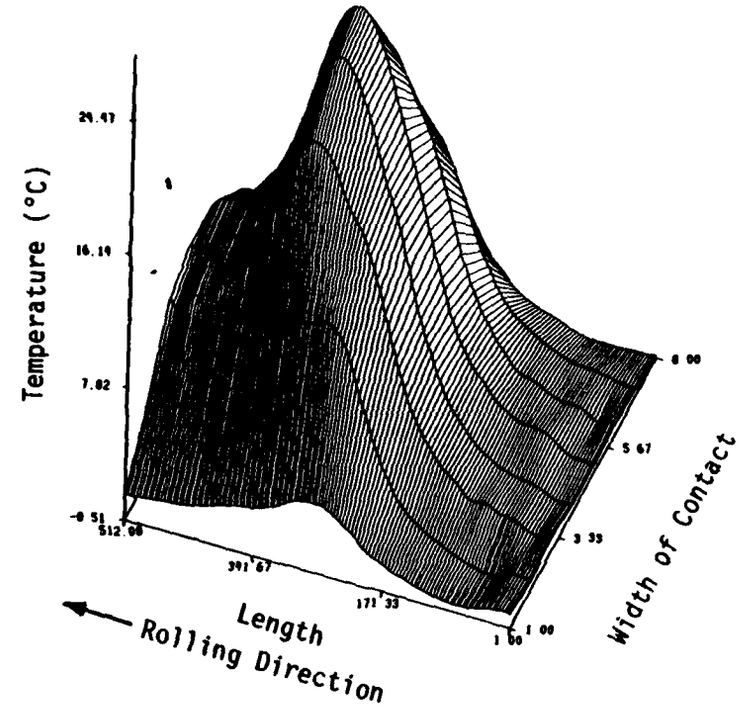

b) Temperature Distribution Above Ambient

Figure 6. Pressure and temperature distribution for 6.2% slip condition.

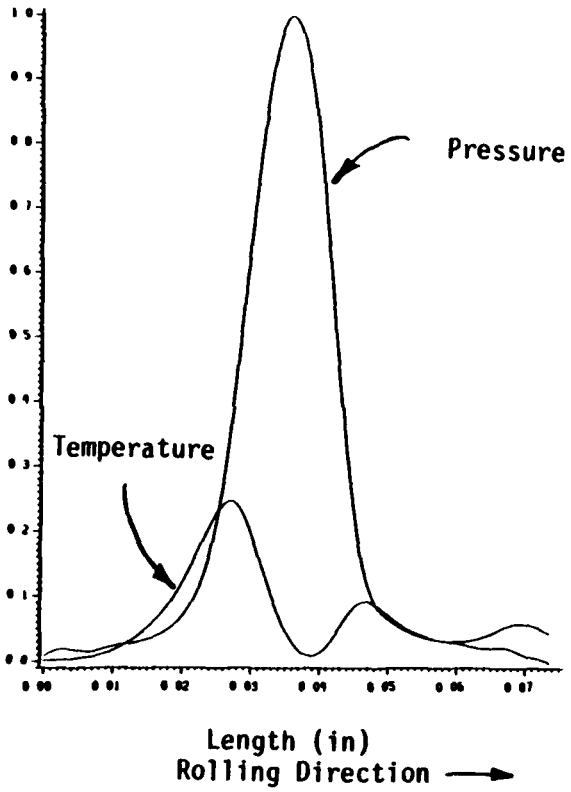

a) Pure Rolling Condition

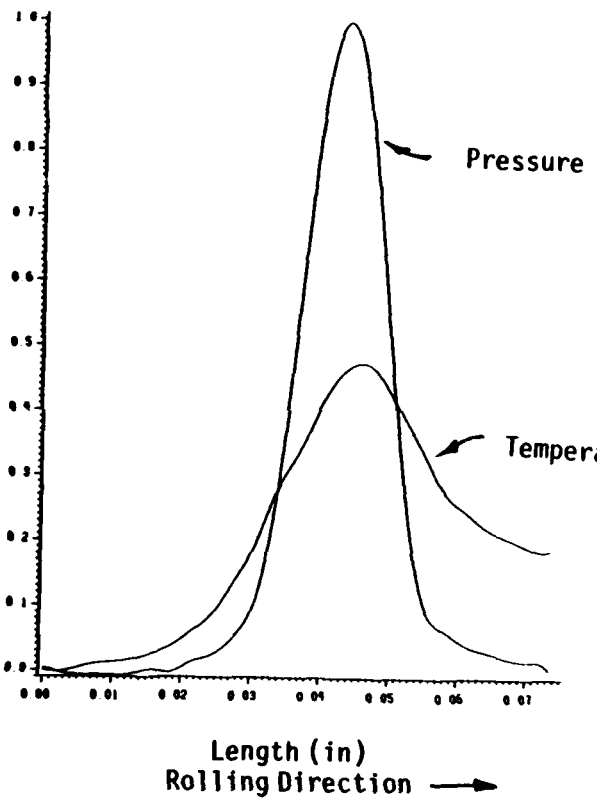

b) 6.2% Slip Condition

Figure 7. Surface pressure and temperature variation through the center of contact (center of width in Figures 5 and 6).

Vertical scale for pressure = psi/250,000
Vertical scale for temperature = °C/50

Table 2. Input Data for Computational Procedures

Input Parameters			Data
Diameter of Disks			1.405 in.
Material of Both Disks			Steel
Rotational Speed			5,000 RPM
Surface Speed			368 in/sec
Lubricant			XRM-109F
$c_f * \rho_f$	~	Specific heat of the lubricant times density	253 $lb/in^2°C$
K_f	~	Thermal conductivity of the lubricant	.054 lb/sec°C
$c_s * \rho_s$	~	Specific heat of the disk times density	540 $lb/in^2°C$
K_{1s}, K_{2s}	~	Thermal conductivity of disk	6.00 lb/sec°C
E_1, E_2	~	Modulus elasticity of disks	$30x10^6$ lb/in^2
ν_1, ν_2	~	Poisson's Ratio of disks	.3
δ	~	Temperature coefficient of lubricant	.04 1/°C
β	~	Thermal expansivity of the lubricant	.00069 1/°C
z	~	Pressure viscosity index	.45

Table 3. Measured Data for Traction and Film Thickness

Peak Hertz Pressure (Ksi)	Lubricant	Disk Temp. °C	Ambient Viscosity cp	Film Thickness $x10^6$ in	Slip %	Traction (lbs)
203	XRM-109F	64	125	73	0.0	0.0
203	XRM-109F	63	110	50	6.2	5.0

Figure 8* illustrates the temperature distribution through the thickness of the film for pure rolling and 6.2% sliding conditions. These temperature distributions were calculated for the fluid in the center of contact where the pressure is the highest. For pure rolling conditions, the peak lubricant temperature rise in the film is 39°C, for the case where the surface temperature peak is 13°C above ambient. For the 6.2% slip case, the peak temperature rise in the film is 152°C for a surface peak of 25°C above ambient. Clearly such changes in temperature must be considered if an accurate prediction of the performance of the contact is required.

Figure 9 contains the components of heat generation due to shear and compression heating which produced the temperature field for the pure rolling condition. For this condition all of the shear heating is generated in the inlet zone. The shear heating is maximum at the disk surface and gradually decreases to its minimum of zero at the center of the film. The shear heating also goes to zero in the contact zone because the velocity gradient is zero for pure rolling. The maximum value for shear heating (68000 lb/in^2sec) occurs at the surface near the entrance to the contact zone. The compression heating and cooling occurs mostly in the contact zone.

The compression heating is influenced principally by pressure gradient but also by temperature, velocity, and coefficient of thermal expansion. Pressure and temperature are moderate in the inlet zone and

---

*Note that this figure differs from Figures 5 and 6. The lateral dimension of Figures 5 and 6 is the width of the contact zone along the axis of the cylinders. In the remainder of the figures in this section the lateral dimension will be the dimensionless film thickness; that is, they will illustrate the temperature and heat generation through the thickness of the lubricant film at the centerline of the width of contact.

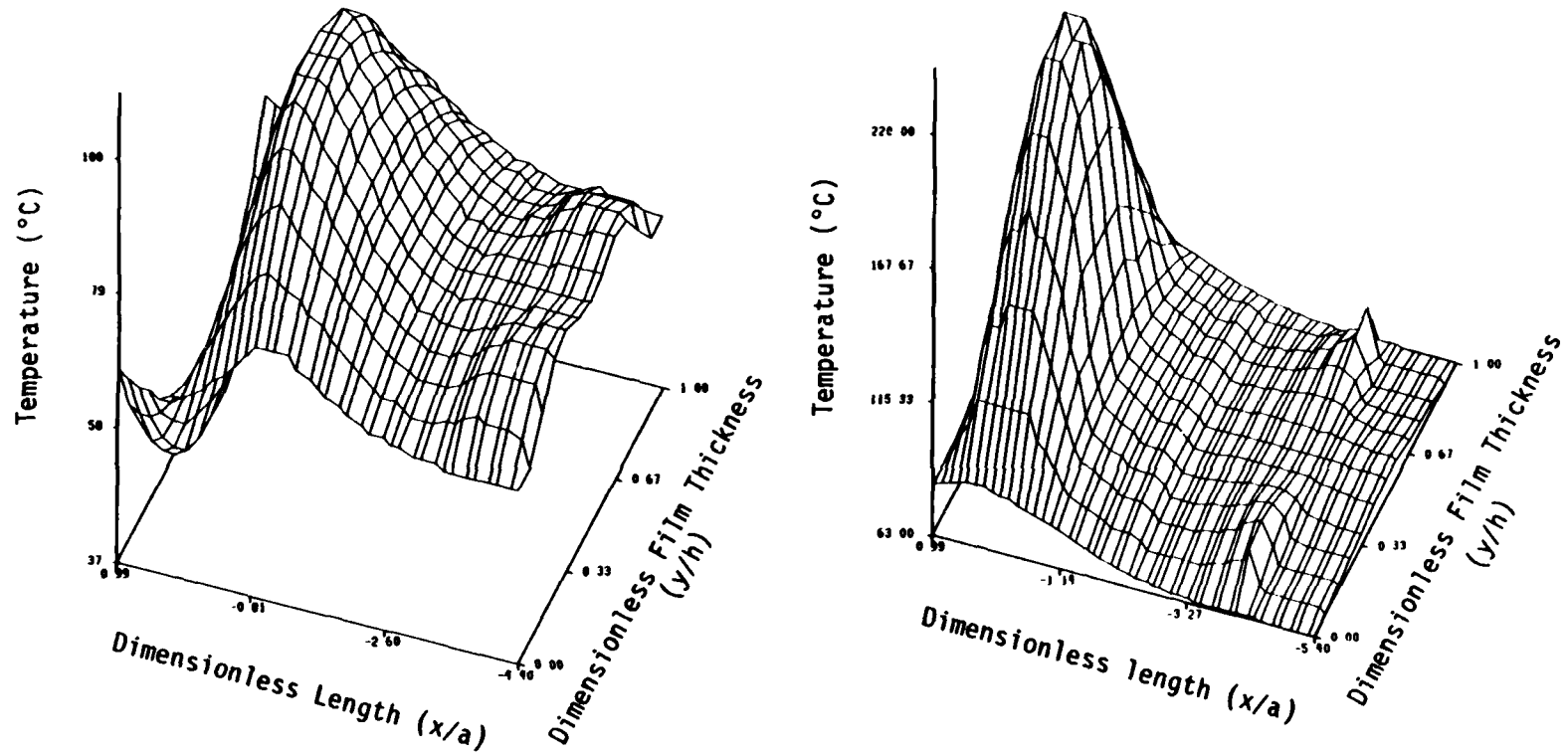

a) Pure Rolling Condition

b) 6.2% Slip Condition

Figure 8. Temperatue distribution through the thickness of the film.

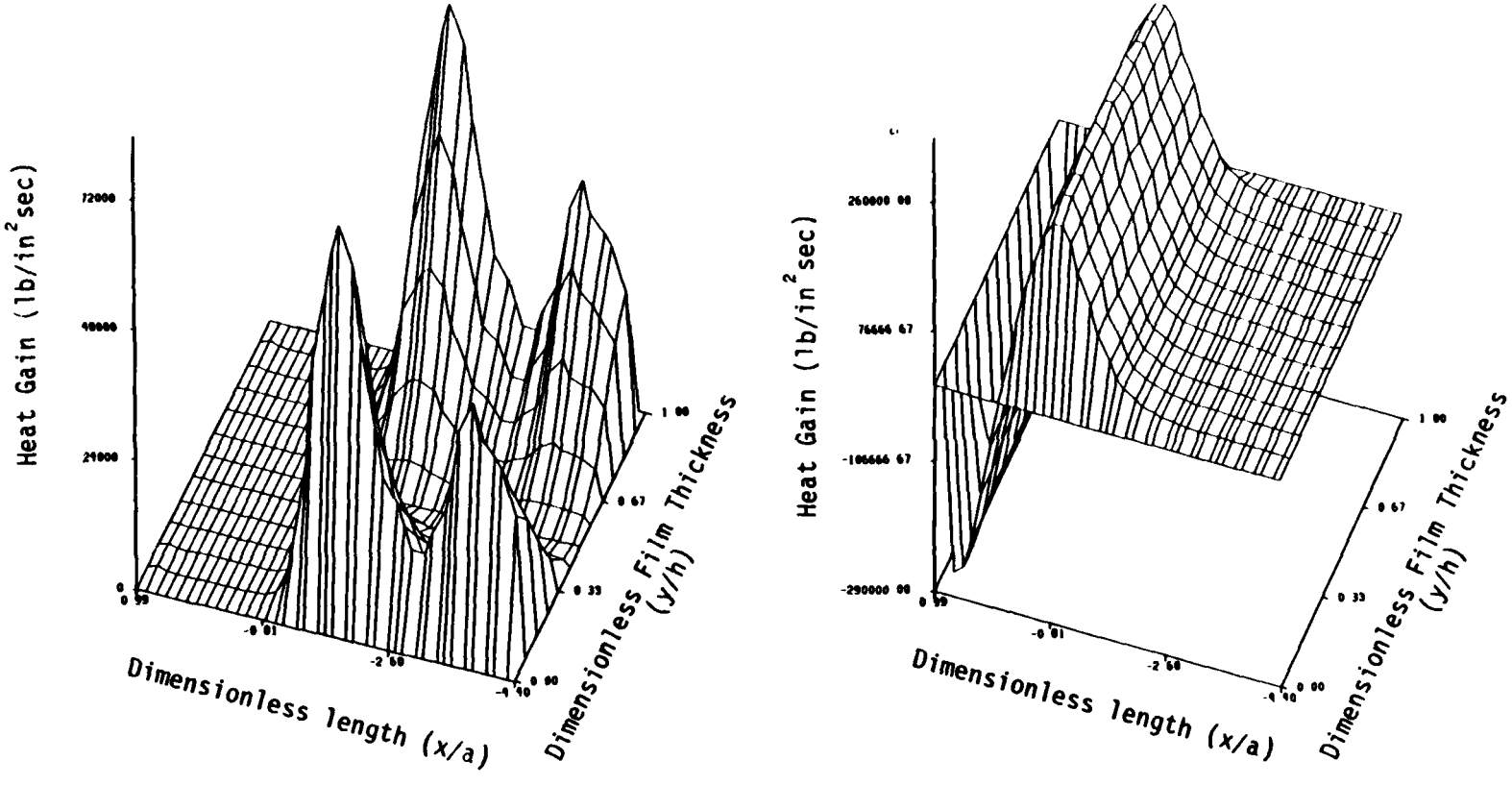

a) Shear Heating

b) Compression Heating

Figure 9. Shear and compression in the film for pure rolling condition.

rise to their maximum values in the contact zone. Compression heating reflects the rate of change and its maximum value of 260,000 lb/in^2sec occurs at the point of maximum presssure gradient. After the peak pressure, the rate of decrease produces a cooling effect on the lubricant film. Compression heating has only a moderate effect on temperature rise in the inlet zone. But in the contact zone most of temperature increase and decrease is due to compression heating and cooling.

Figure 10 represents the heat loss due to conduction and convection across the lubricant film. Most of the heat generated in the contact is lost by conduction. This conclusion follows from a comparison of figures 10 (a) and (b). The peak value of conduction is 250,000 lb/in^2sec and its shape is nearly the inverse of the heat generation due to compression. The maximum convection loss in the x-direction is about 1/10 of the conduction and is out of phase; that is, the maximum gain of heat in an element of the film due to convection occurs near the point of maximum loss due to conduction.

The convection in the x-direction has peak values in the center of the contact where the velocity and the temperature gradient in the x-direction are the greatest. The convenction in the y-direction has maximum values at the boundaries of the film, that is, the disk surfaces as shown in Figure 11. This convection term is proportional to the velocity and temperature gradient in the y-direction, the density, and specific heat of the lubricant. This term vanishes at the center of the contact where the y-component of velocity goes to zero because of symmetry and the contact zone where the x-component of velocity is dominant.

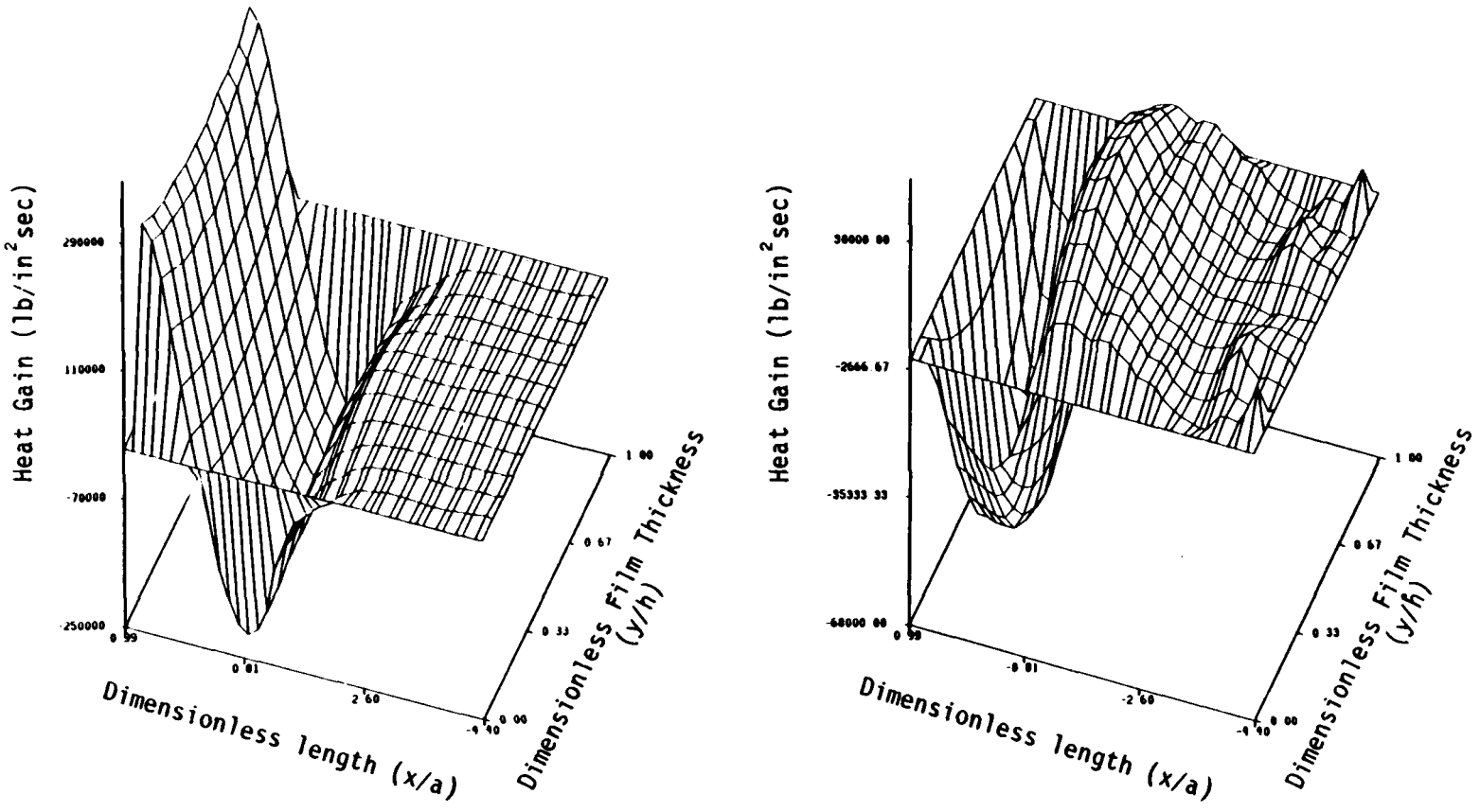

a) Conduction Heating

b) Convection (x-direction) Heating.

Figure 10. Conduction and convection in the film for pure rolling condition.

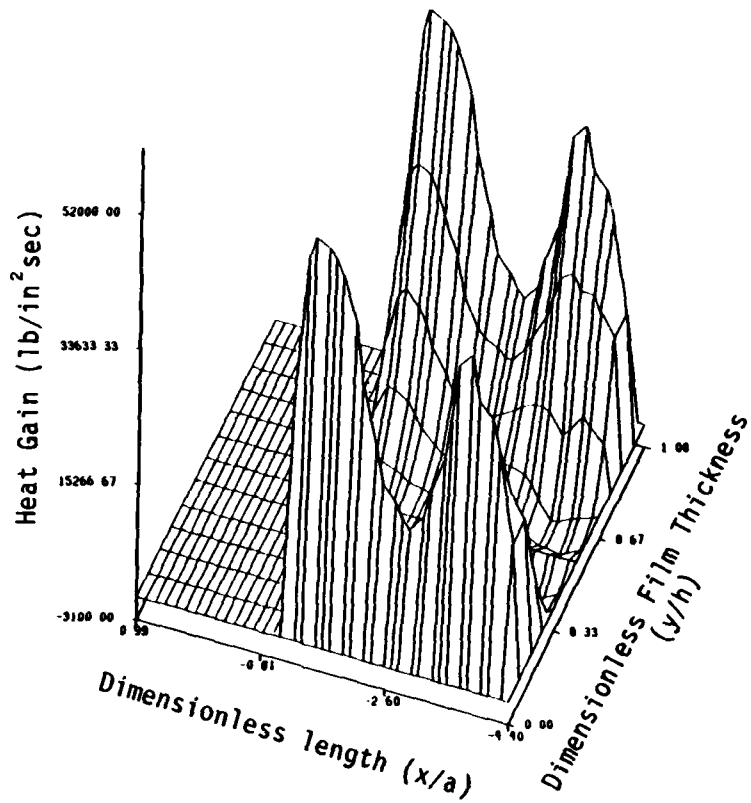

Convection (y-direction) Heating

Figure 11. Convection (y-direction) heat loss in the film for pure rolling condition.

Figure 12 illustrates the shear and compression heating components for the 6.2% slip case. For this case, in contrast to pure rolling, most of the heat is the result of shear heating, and it occurs in the high-pressure contact zone. The maximum value is 5,200,000 lb/in^2sec or 75 times that of pure rolling. Significant shear heating also occurs in the inlet zone, but compared to the peak value, it does not appear on the graph. The compression heating and cooling are similar to the pure rolling case. However, because the shear heating due to slip is so large, the compression term has less effect on the temperature in the film.

The conduction heat loss for the slip case is shown in Figure 13. As in the case of pure rolling, it is the dominant mode of heat transfer. The conduction heat loss reaches it maximum value of (5,100,000 lb/in^2sec) in the contact zone and it appears almost identical to the shear heat gain in the film. The convection heat loss in the x-direction for the slip case (Figure 13) is also similar to the case of pure rolling, but its magnitude (220,000 lb/in^2sec) is sharply increased due to the sharp increase in temperature gradient in the x-direction. Figure 14 shows the heat convection in the y-direction for 6.2% slip case. It is of the same general shape as in the case of pure rolling, but its magnitude (86,000 lb/in^2sec) has moderately increased. This moderate increase is due to an increased temperature gradient in the y-direction.

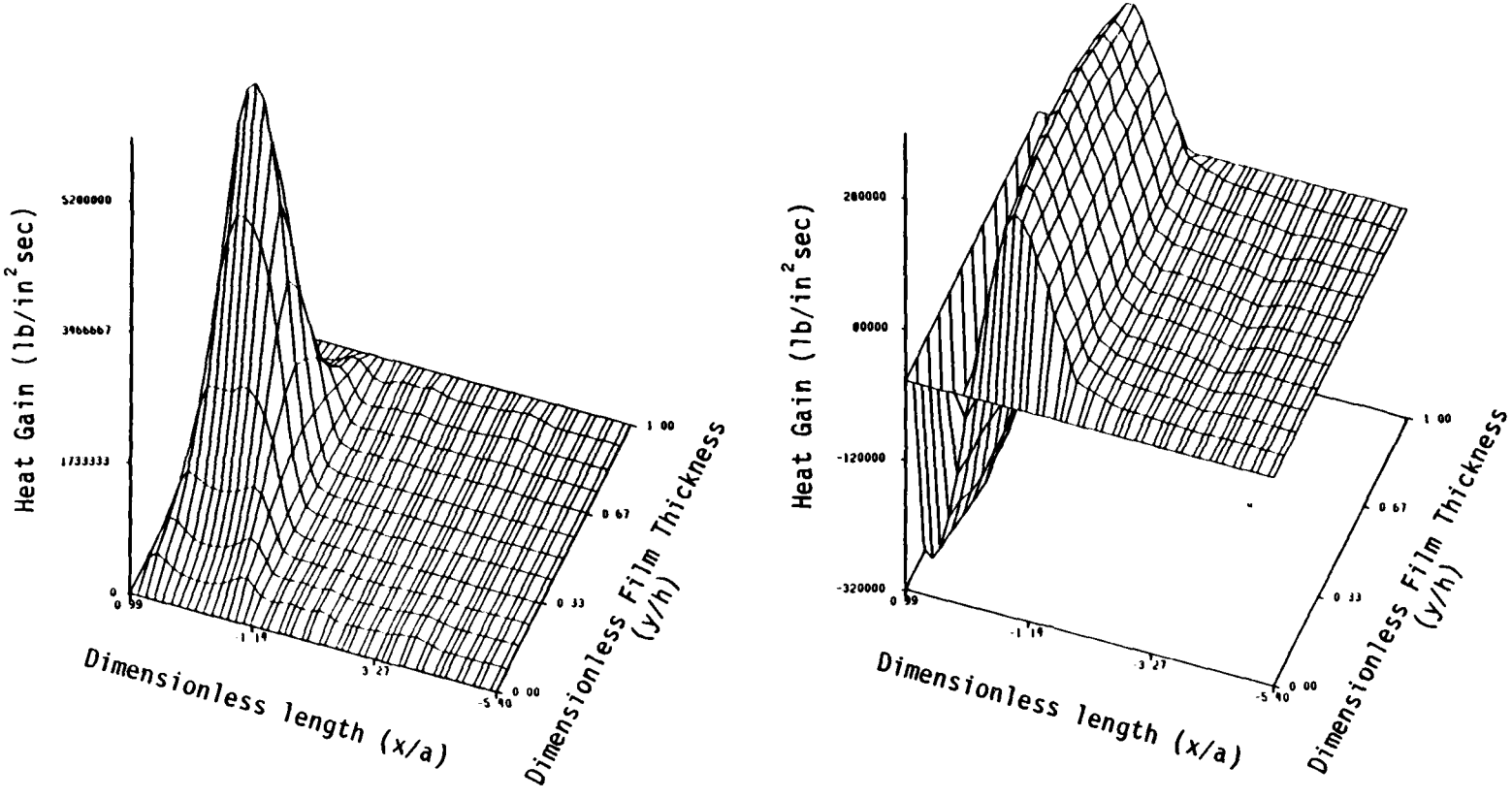

a) Shear Heating

b) Compression Heating

Figure 12. Shear and compression in the film for 6.2% slip condition.

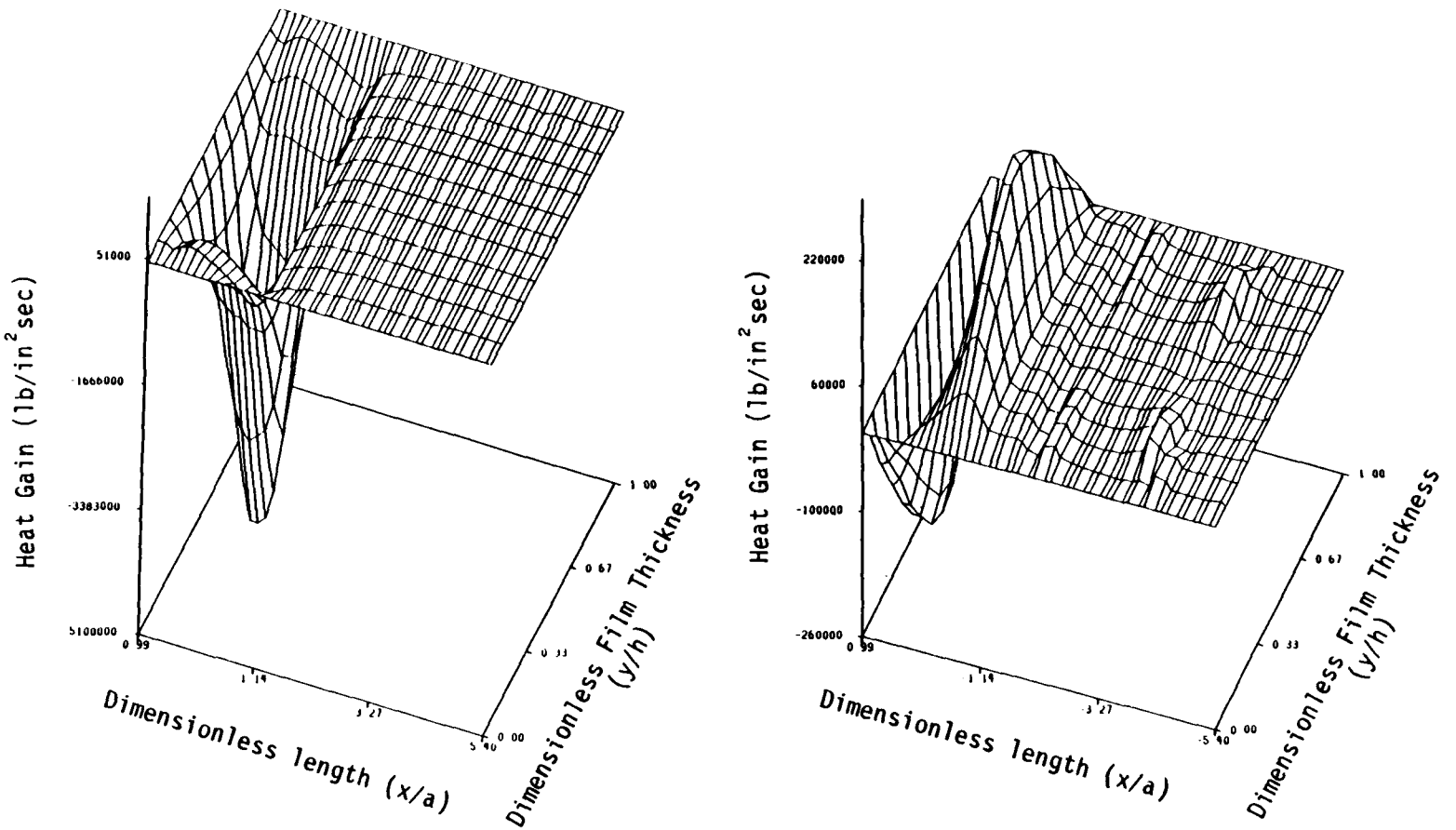

a) Conduction

b) Convection (x-direction) Heating

Figure 13. Conduction and convection in the film for 6.2% rolling condition.

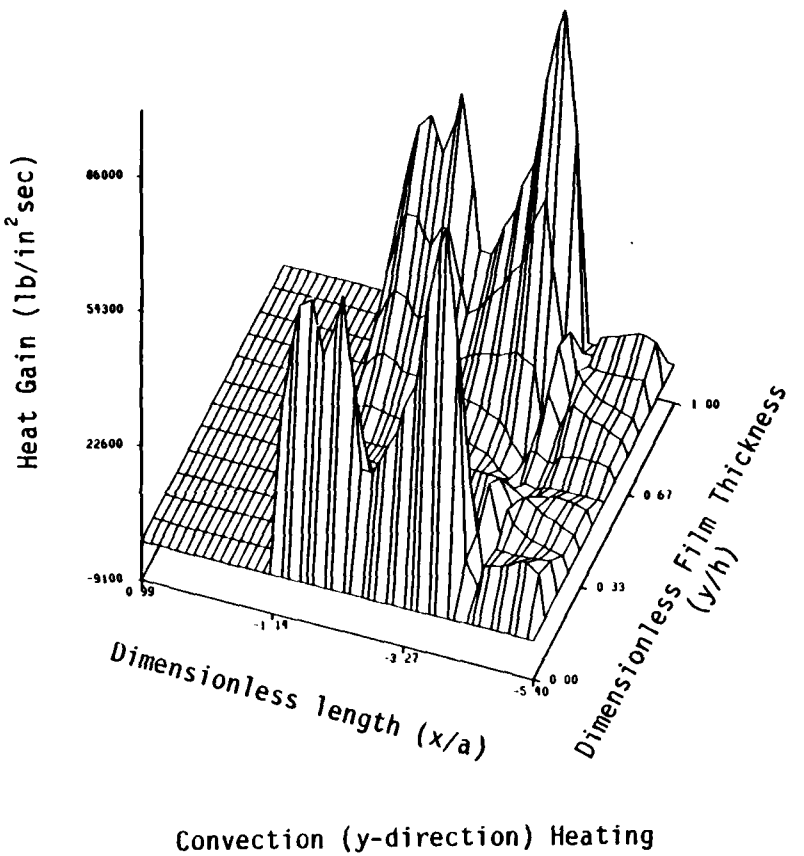

Figure 14. Convection (y-direction) heat loss in the film pure rolling condition.

Electrical Brush Contact

The objective of this task of the program was to develop a model for wear of high-current-density electrical brushes. Experimental measurements were performed and used to corroborate the postulated model.

Experimental Apparatus

To study the contact phenomenon which occurs in high current density electrical brushes, the apparatus shown in Figure 15 was constructed. This apparatus consists of a 100 mm diameter copper slip-ring supported in ball bearing pillow blocks. The slip-ring was belt driven at speeds up to 5000 revolutions per minute producing a surface velocity of 26.6 m/sec (1000 in/sec).

The brush was mounted in a copper holder pivoted about an axis parallel to the slip-ring axis as shown in Figure 15. This provided for vertical motion of the brush which was dead weight loaded onto the slip-ring. The preloaded ball bearing pivot prevented unwanted horizontal motion of the holder. Angular adjustment of the brush was allowed to permit operation with either a leading or trailing angle with respect to the slip-ring motion. For all of the cases reported here, the brush was operated in a seven degree leading configuration. To minimize the dynamic effects produced during operation, the brush holder was connected to a viscous damper through a lever arm.

The brush samples had a contact region of 25 mm (1.0 in) by 2.5 mm (0.1 in) to produce an appararent contact area of 0.645 cm^2 (0.1 in^2). Current was supplied to the apparatus by a DC Power Supply capable of delivering a maximum of 100 amperes. With this arrangement, current densities up to 1.56 M-amperes/m2 (1000 amperes/in2) were possible.

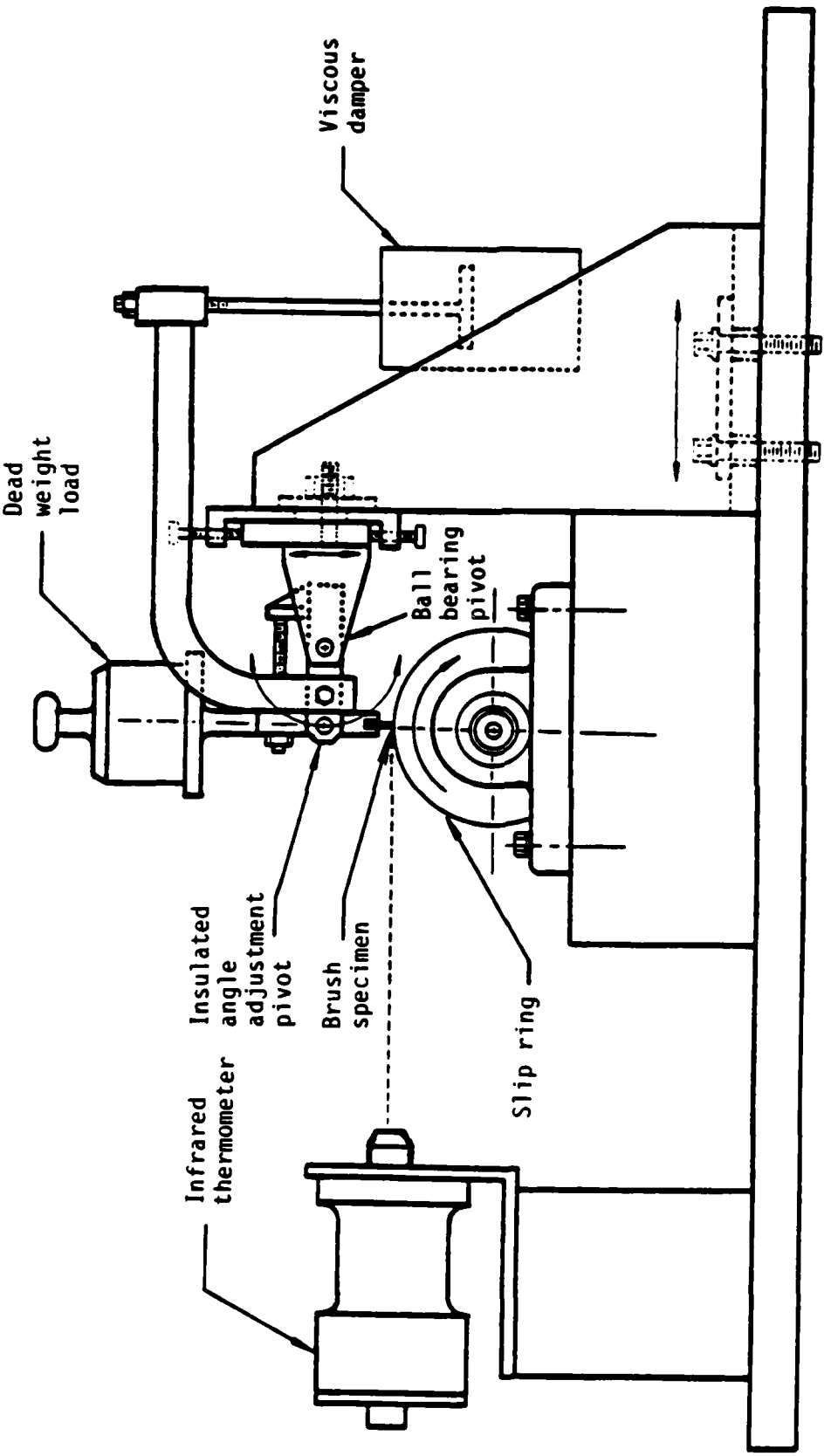

Figure 15. Layout drawing of experimental apparatus.

All tests were run with an anodic brush; that is, the brush was connected to the positive terminal of the power supply. Current was returned from the rotor to the negative power supply through several conventional, spring loaded electrographitic brushes The total return brush area was kept large to minimize the current density and wear of these brushes. All of the tests were performed in ambient air having an approximate temperature of 21°C and 45 percent relative humidity.

Instrumentation

The apparatus was equipped to measure the following quantities:

1. Brush & Slip-Ring Motion -- Two eddy current proximity probes were mounted to read the vertical motion of the brush and the slip-ring runout. These probes were extremely sensitive and capable of reading 0.1 micrometer displacements with a bandwidth above 100 Kcycles.

2. Voltage Drop -- The voltage drop produced across the brush slip-ring interface was measured through an auxiliary brush mounted to the right of the brush sample. This brush was external to the current path and thus not subject to the effects of Joule heating. Voltage drop could be measured simultaneously with current flow, brush motion, and slip-ring runout.

3. Current Flow -- The instantaneous current was monitored by measuring the voltage drop across a fixed resistance in the supply line.

4. Temperatures --The brush bulk temperature and interface temperature were measured. The bulk temperature was obtained by placing a thermocouple in the base of the brush at a distance of approximately 6 mm (0.25 inches) above the contact surface. The interface temperature was determined by using an infrared temperature detector. This device

optically monitored a 0.9 mm diameter spot near the interface with a response time of approximately 100 milliseconds. It was sensitive to temperatures between 150°C and 800°C.

5. Sparking --The presence and intensity of sparking was measured through the use of a photo-darlington (photo-transistor). This device was mounted behind the brush and in close proximity to the brush/slip-ring interface. It was relatively free of the effects of radio frequency noise and produced an output between zero and twelve volts for sparks intense enough to trigger its gate.

Wear Tests

To examine the effects of material properties and operating conditions on brush wear, a series of experiments were performed. Four electrographitic brush materials were examined. The properties of these materials are presented in table 4. The brush loads utilized were 4.5 and 9 Newtons. Wear tests for zero current were performed to determine a baseline for electrically induced wear.

The results of the wear tests are presented in terms of the wear coefficient in the Archard wear law [8]. This model assumes that the wear volume is proportional to the load and the sliding distance. The wear coefficient is the constant used to relate the operating conditions to the wear volume. The wear volume (V_w) can be written as:

$$V_w = C_w L D \tag{9}$$

where C_w = wear coefficient (length^2/force)

L = load

D = sliding distance

TABLE 4

Material Properties of Brush Grades
(Vender Supplied Data Except as Noted)

Grade	Contact Hardness (10^6 N•m^{-2})	Flexure Strength (10^6 N•m^{-2})	Density (g•cm^{-3})	Electrical Resistivity (10^{-6} Ω•cm)	Thermal Conductivity (Watt•cm^{-1}•°K^{-1})	Heat Capacity (Watt•s•cm^{-1}•°K^{-1})
L1	1.0	17.2	1.59	10	0.85	1.32
W417	2.0 *	15.2	1.61	17	0.17	1.33
124	1.8	20.7	1.50	46	0.13	1.26
161	1.5	15.2	1.39	56	0.13	1.15

*Experimental Data

The wear coefficient for each material as a function of current is shown in Figure 16 for a specific load and speed. The wear coefficient at no current was approximately the same for all of the brush materials studied and was small compared to that measured in the current tests. A non-linear increase in wear coefficient was measured as the current density was raised and the magnitude of the increase was very material dependent.

Two obvious regimes of wear were observed during the tests; that for sparking and non-sparking operation. The key parameter was the rotating speed of the slip-ring. At low speeds (1620 rpm) no sparks or hot spots were observed on the brush face and the wear of the brush was low. However, as the speed was raised to 2750 rpm, hot spots were observed and a much higher value of wear coefficient was measured. This behavior is illustrated in Figure 17 for the four brush materials at a fixed value of current density and load.

For a given operating speed and current density, the wear coefficient was constant and independent of sliding distance for any brush material. This indicated that the wear behavior obeyed Archard's wear law in that respect.

For the low speed case in Figure 17, no sparking was observed and the wear coefficients for the test materials ranged between 10^{-9} and 10^{-10}. At the higher speed heavy sparking was observed and the wear coefficient increased by approximately an order of magnitude for each material. Figure 18 shows a similiar comparison except at double the brush load of Figure 17. The effect of increasing the load is to reduce the wear coefficient. This result is contrary to the Archard model but, because a dead-weight loading system is used, the increased load also affects the dynamics of the brush motion. This effect will be discussed further in the section on wear model development.

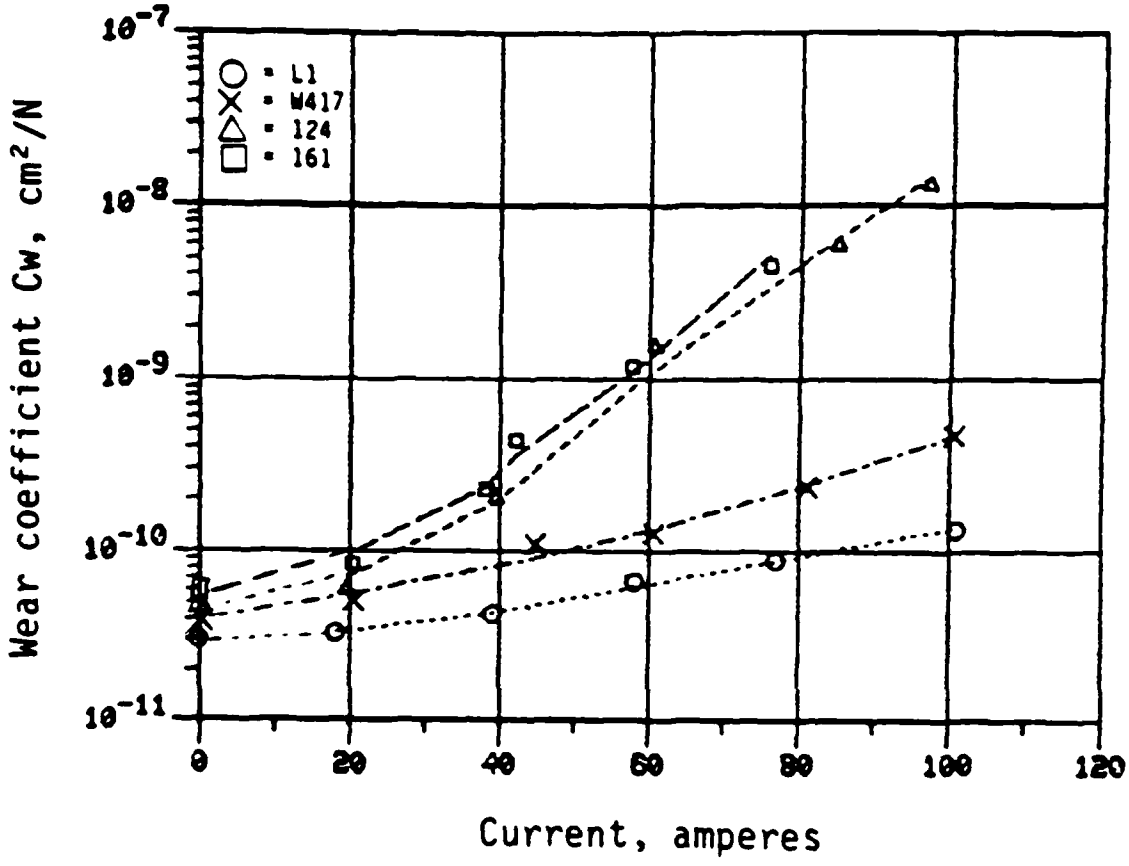

Figure 16. The variation in the wear coefficient with the current passage, 4.5 N load, 1620 rpm.

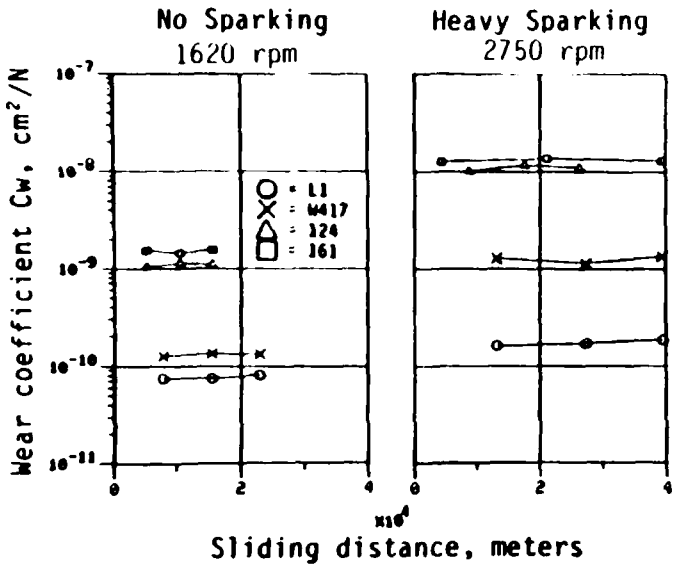

Figure 17. The effects of sparking on the wear coefficient, 4.5 N load, 9.3×10^5 A/m^2.

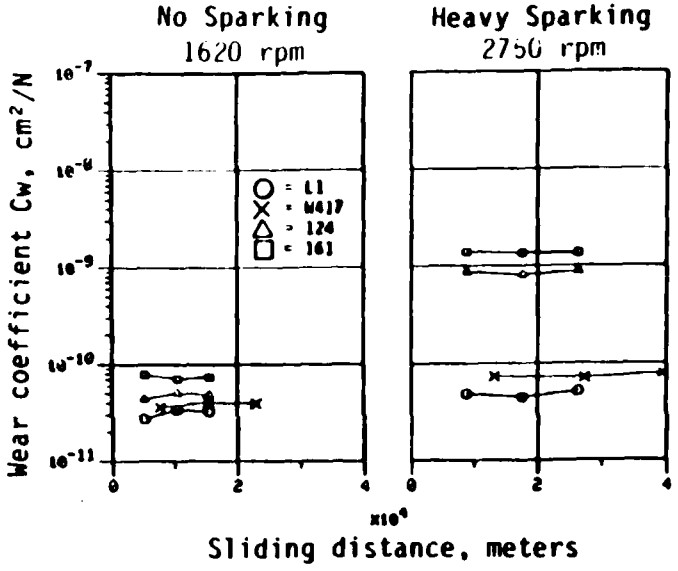

Figure 18. The effects of sparking on the wear coefficient, 9 N load, 9.3×10^5 A/m^2.

The results of the wear tests indicated that the brush wear increased with the current density and speed and decreased with dead-weight load. The brush material properties also played a significant role in the wear process. The role of the brush properties will be considered next.

Analysis of Wear Test Results

Figures 17 and 18 show a ranking in wear of the four materials which is consistent for all the operating conditions studied. The lowest wear occurs for the grade L1 and the highest for grade 161. From a comparison of the material properties of these brushes, a parameter which showed a similiar relationship was the ratio of electrical resistivity to thermal conductivity (r/k). The ratio fits well with the hypothesis that the wear is related to hot spots on the brush surface. The heat generation due to the constriction resistance is proportional to the resistivity, and the removal of that heat will be proportional to the conductivity. A high value of this ratio will occur for a material with high resistivity and low conductivity, a combination which should produce local high temperatures. Table 5 shows this ratio for the four brush materials and the corresponding wear coefficient at 4.5 N load and 1620 rpm. In all cases, the r/k ratio is nearly proportional to the wear coefficient.

TABLE 5

Relationship Between Wear Coefficient and (r/k) Ratio

Brush Grade	Wear Coefficient	r/k
L1	8×10^{-11}	1.2×10^{-3}
417	15×10^{-11}	10.0×10^{-3}
124	100×10^{-11}	35.4×10^{-3}
161	150 x 10-11	43.1 x 10-3

Table 6 presents the voltage drop measured for the wear tests of Figures 17 and 18. This table shows that the voltage drop increases in proportion to the electrical resistivity of the brush material. It also shows that increasing the brush load reduces the voltage drop. These observations could be a result of the relationship between load and contact area. Since the voltage drop occurs chiefly across the constriction resistance, an increase in resistivity would increase the voltage drop for a given load. However, increasing the load will produce a larger contact area and reduce the constriction resistance leading to a lower voltage drop.

Table 7 indicates that significantly different bulk and peak interface temperatures were measured for the different brush materials. The brush materials are presented in this table in ascending order of their (r/k) ratio from left to right. The temperature measurements indicate those materials with a higher r/k ratio exhibit higher bulk and interface temperatures for the same operating conditions. Table 7 also shows that the bulk temperature of the brushes are nearly the same for operation with and without sparking. However, the interface temperature is significantly larger for operation under sparking conditions. This indicates that the high temperature exist only near the interface.

The results of the wear test are consistent with the hypothesis of local hot spots at the contact regions. However, the appearance of the hot spots at high rotation speeds suggest that brush dynamics play an important role.

TABLE 6

Operational Voltage Drops for the Brush Materials
(9.3×10^5 A/m^2)

		1620 rpm		2750 rpm	
		4.5 N	9 N	4.5 N	9 N
Brush Grade	Electrical resistivity (10^{-3} Ω·cm)	Voltage Drop		Voltage Drop	
L1	1.0	1.17	0.93	1.68	1.04
W417	1.7	1.21	0.87	2.24	1.11
124	4.6	1.77	1.37	3.04	1.68
161	5.6	2.13	1.60	2.95	1.88

TABLE 7

Operational Temperatures for the Brush Materials
(9.3×10^5 A/m^2)

			Brush Grade			
Speed	Parameter	Load	L1	W417	124	161
No Sparking 1620 rpm	Bulk Temperature (C)	4.5 N	89	96	154	163
		9 N	79	82	107	118
	Peak Interface Temperature (C)	4.5 N	-	-	416	482
		9 N	-	-	-	177
Sparking 2750 rpm	Bulk Temperature (C)	4.5 N	91	106	168	171
		9 N	79	82	129	143
	Peak Interface Temperature (C)	4.5 N	-	232	577	682
		9 N	-	-	416	454

Sparking Tests

Shobert and Jones have suggested that sparking is caused by contact separation resulting from brush dynamics [4,9]. They surmised that separation could result in the production of an arc or plasma which are the visible "sparks." To study the nature of "sparking" and the relationship between brush motion, voltage drop, current flow and the appearance of a "sparking," a series of experiments was performed. Tests were conducted with both moving and stationary slip-rings while the brush displacement, voltage drop, current flow, and photo-darlington output were monitored.

Static Tests

The static sparking tests were conducted to observe the electrical circuit behavior without the complications introduced by machine dynamics. The results of these tests are later compared to those obtained in the dynamic tests to determine if sparking was produced only by contact separation.

Figure 19 shows the voltage drop (upper trace at left) and the brush displacement (lower trace) during such a test. While in a static contact with the copper rotor, the W147 brush experienced a voltage drop of 1.2 volts. As the brush was lifted, the voltage drop gradually increased. When the voltage approached a limiting value of four volts it stabilized momentarily and then jumped toward the open circuit potential of thirteen volts. During the rise of the voltage from four volts to the open circuit value, rapid oscillations of the current and voltage were observed. Figure 20 shows the behavior of the voltage drop (lower trace) and photo-darlington output (upper trace) respectively during such a

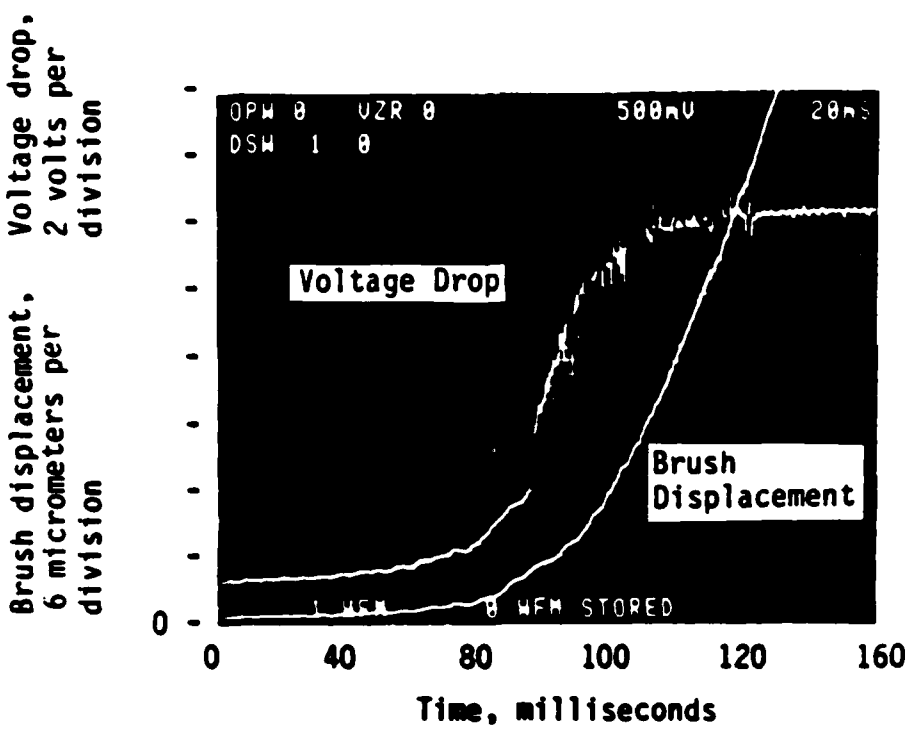

Figure 19. Relative brush displacement and voltage drop behavior during brush lifting tests, W417 brush, stationary rotor, 4.5 N load, and 9.3×10^5 A/m^2.

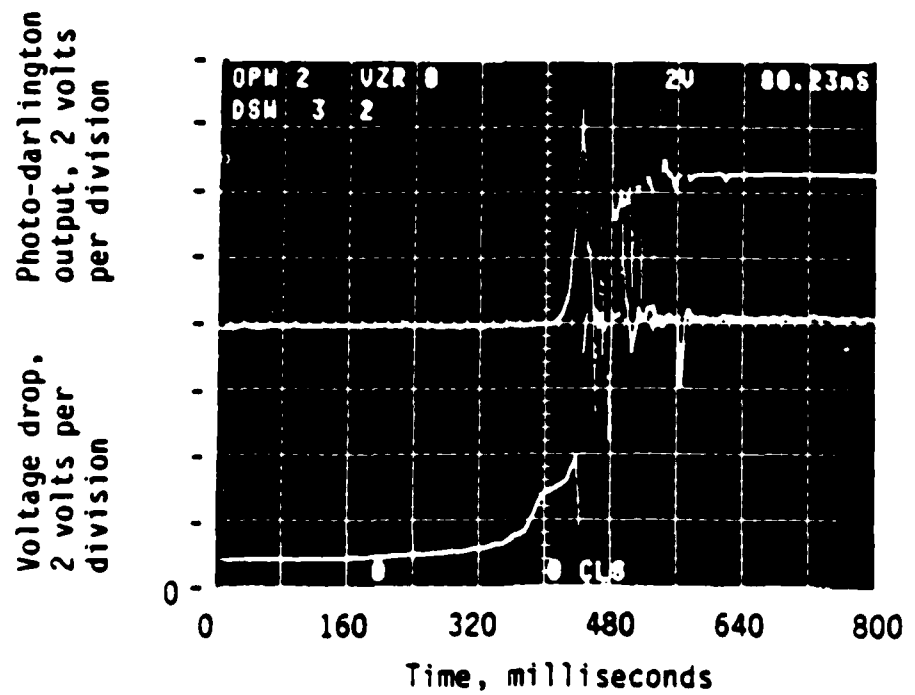

Figure 20. Voltage drop and photo-darlington behavior during brush lifting tests, W417 brush, stationary rotor, 4.5 N load, and 9.3×10^5 A/m^2.

test. At the point of the voltage jump a large output of light was observed and recorded as a spike in the photo-darlington output. The brush had a relative displacement of approximately 6 micrometers when this occurred. Regardless of the lift speed used this behavior was consistent. With slower lift speeds, however, extensive heating of the contact surface was evidenced by intense visible light and high output from the photo-darlington.

The voltage drop measured in these tests increased as a function of relative brush displacement. This behavior could occur if the surfaces were in contact and the reduction in load reduced the size of the contact spots, or if separation actually existed and the current was moving through an arc or plasma.

A second series of tests was performed to clarify this question. These tests involved beginning with the brush out of contact and slowly lowering it toward the slip-ring. During these tests it was observed that the voltage drop and current flow experienced the same type of oscillations as were seen for the lift tests. Figure 21 shows the voltage drop (upper trace) and the brush displacement (lower trace). As the brush approaches within 0.05 mm of the slip-ring, oscillations in the voltage drop were observed. Jones indicates that the development of an arc or plasma occurs after thermal activation of the contact surface [9]. Such thermal activation requires the passage of some current in the presence of a potential. As the brush was being dropped cold onto the slip-ring from a zero current condition, no thermal activation of the contact region could have yet occurred. The implications of these tests were that the voltage or current oscillations observed were not due to the development of a plasma, but that deviation in the surface profile of the brush and slip-ring reduced the observed gap. This reduction in the

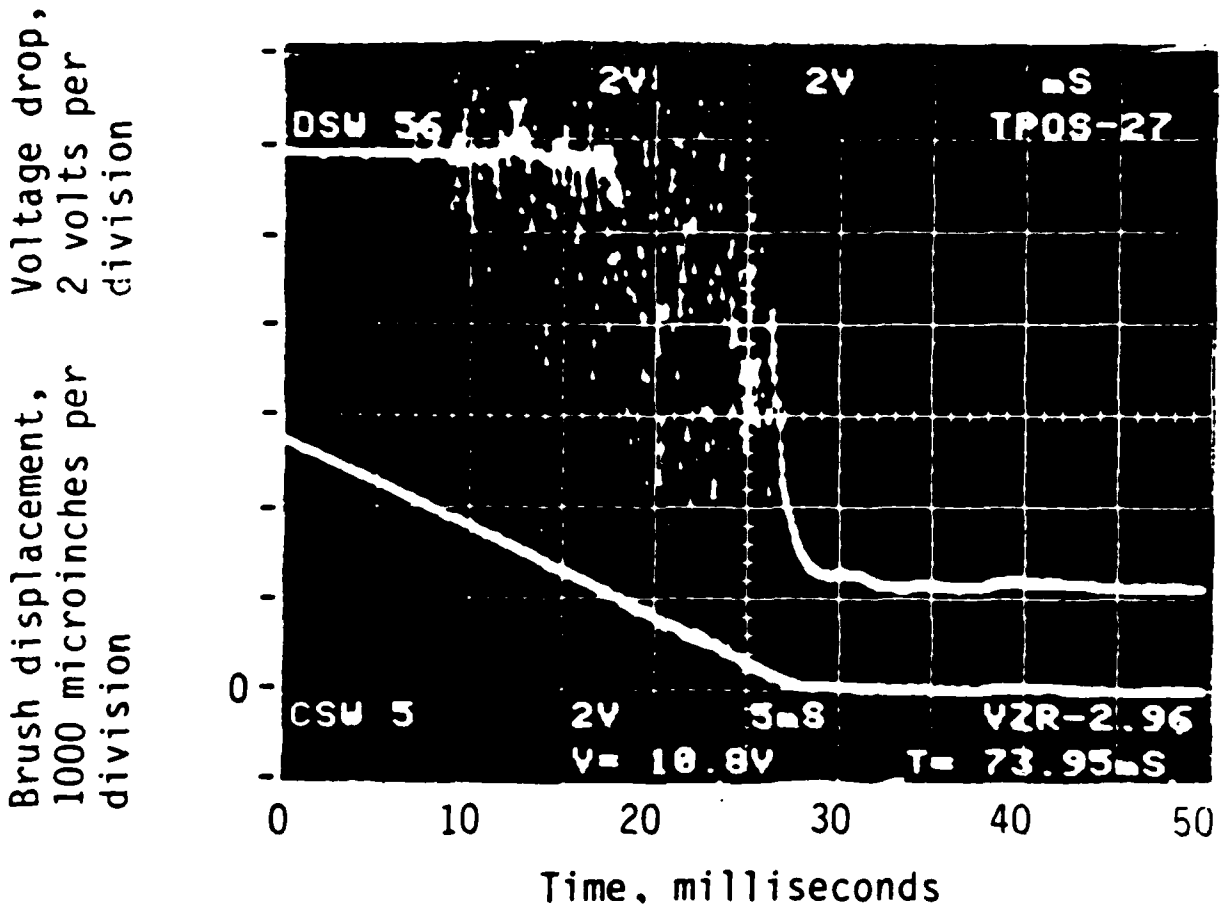

Figure 21. Relative brush displacement and voltage drop behavior during brush drop tests. W417 brush, stationary rotor, 4.5 N load, and 9.3x105 A/m^2.

gap resulted in a dielectric breakdown of the air or the contact of asperity peaks and thus produces the oscillations. Once the relative displacement indicated 6 micrometers, the current passage and voltage drop stabilized and quickly approached the static value of 1.2 volts.

Dynamic Tests

Dynamic tests were performed to correlate the observations made during the static tests to the electrical behavior of the apparatus during sparking operation. Speeds of 1000 rpm and greater were examined in these tests.

It was found in these tests that no sparking was detected below 1700 rpm. At 1000 rpm the voltage drop across the interface using a W417 brush was nearly constant at 1.2 volts and no sparking or hot spots were observed. At higher rotational speeds the voltage drop developed peaks which measured above 3 volts and sparks were observed. (See Figure 24). Further increases in speed produced higher peak voltages but these did not exceed six volts. In contrast to the static tests, the potential did not approach thirteen volts after a spark; but rather it dropped to the steady state value.

The brush displacement during these tests was examined for comparison to that observed in the static tests. However, unlike the static tests, the dynamic tests did not have a fixed spacial frame of reference due to the rotational runout of the slip-ring. Therefore, a technique to determine the motion of the brush relative to the slip-ring was developed. To obtain an accurate picture of the relative motion of the brush, the runout of the slip-ring was measured and subtracted from the brush motion. The runout probe was located in the wear track 15 mm ahead of the brush. The error introduced by this placement was corrected

by simultaneously digitizing the probe outputs, shifting them in time to account for their relative positions, and then subtracting them to yield the relative displacement of the brush.

Tests conducted using a W417 brush, (4.5 N load, at a current density of 9.3×10^5 A/m^2) indicated that below 1400 rpm the peak-to-peak amplitude of relative motion was less than 3 micrometers. As the speed approached the maximum of 2750 rpm this amplitude grew to approximately 6 micrometers. At these higher speeds, sparking was observed and moved in clusters with periodic motion across the brush face. The relative displacement for which sparking was observed during the static tests was also approximately 6 micrometers.

To determine if the brush and slip-ring actually separate, the magnitude of brush acceleration was investigated as well as its shape relative to the voltage spikes. The acceleration was obtained from the relative brush displacement by numerical differentiation. Figure 22 shows the acceleration of the brush and the dynamic voltage drop under conditions where sparking was observed. The acceleration varies between $\pm$ 250 cm/sec^2 and the voltage drop has a steady value of about 1 volt with occasional peaks above 3 volts. By comparing these simultaneous measurements, one can observe that the peaks in voltage drop correspond to the maximum values of negative acceleration. This means that the voltage peak occurs when the dynamic loading is reduced by inertia forces due to brush assembly runout. Using the values of peak acceleration shown in Figure 22 with the vibrating mass of the assembly (6.75 Kgm), the inertia force is about 70 percent of the applied load. This would not be sufficient for complete separation to occur.

The form of the peaks in the brush voltage drop is also an important indication of brush/slip-ring contact. Typically, this voltage peak

consisted of an initial rapid increase in voltage (on the order of 200 volts/second) with a peak occurring at approximately four volts. After the voltage peak, the potential would fall approximately one volt and begin climbing again at a rate which was similar to that observed for an open circuit. The top trace in Figure 23 shows the voltage increase when the brush is rapidly separated from a stationary rotor. The dynamic voltage drop for operation at 2750 rpm is shown in the bottom trace. Once past the peak in the dynamic voltage drop the rate of increase of the static and dynamic potentials (the slopes of the two traces) are equal. Thus, it would appear that separation of the brush and slip-ring occurs during dynamic operation. However, the results of the force balance indicated that at the maximum test speed (2750 rpm) the contact load was reduced but not eliminated.

One senario which is consistent with the observations is as follows: The inertia forces reduce the brush loading and, as a result, the contact area. This effectively increases the current density and the temperature of the contacting asperity. When the temperature reaches a critical value, the strength of the material is reduced and a hot wear particle is ejected. Because the debris is visible, the temperature is estimated to be over 2000°C. Such a wear particle would be observed as a "spark" or "hot spot" and could cause a momentary open circuit. Therefore, the voltage drop signal would exhibit the characteristics of a dynamically induced separation without the necessary inertia forces. The next section will consider the consequences of these dynamic effects on the wear of brushes operating at high current densities.

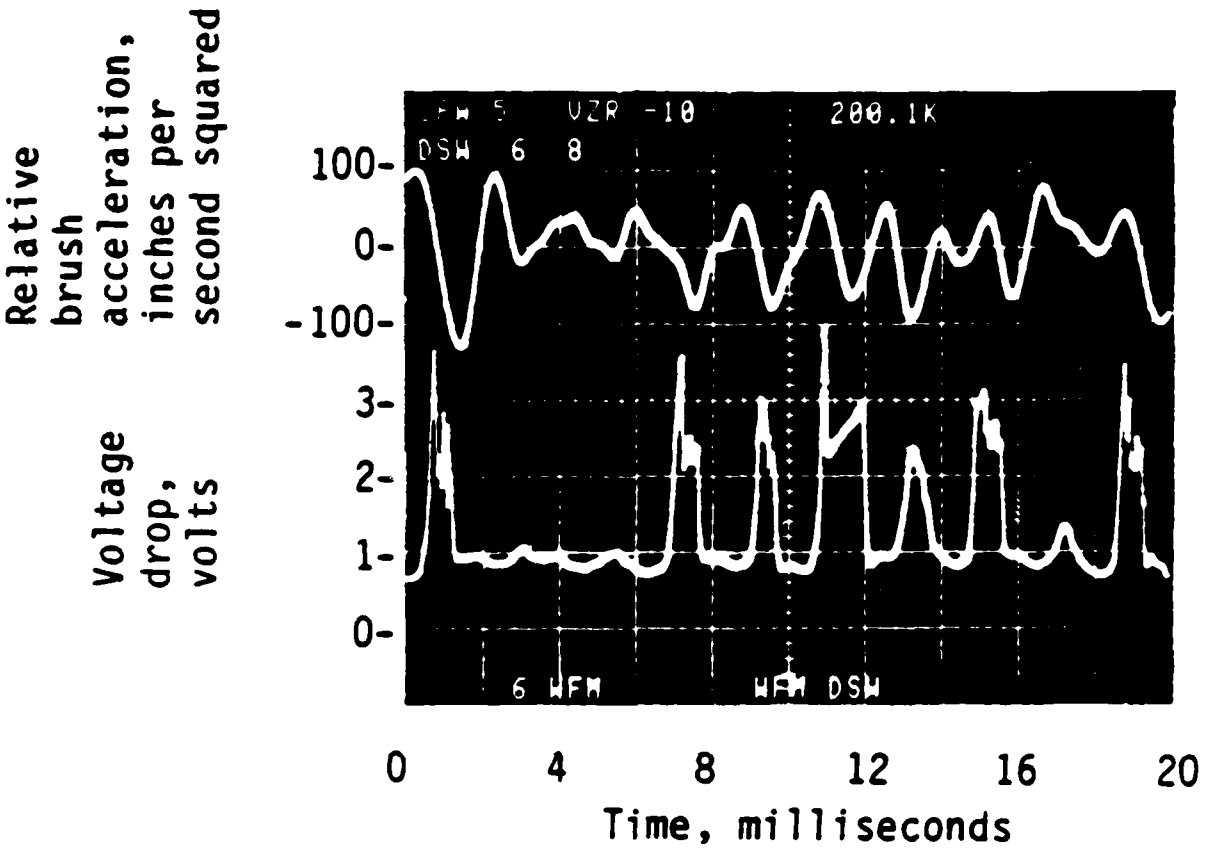

Figure 22. Relative brush acceleration and voltage drop variations with time, W417 brush, 4.5 N load, and 9.3×10^5 A/m^2.

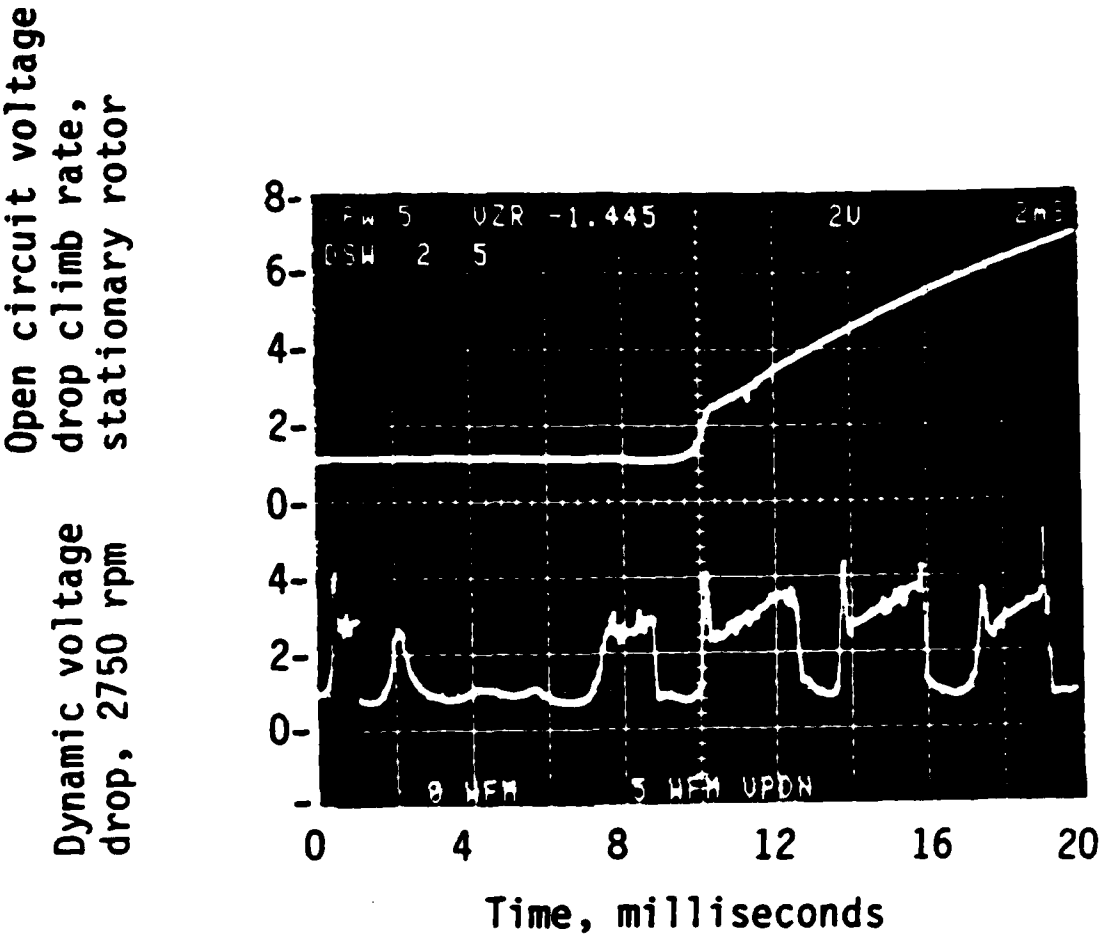

Figure 23. Voltage drop climb rates, W417 brush, 4.5 N load, 9.3×10^5 A/m^2.

Theoretical Model For Brush Wear

The results of the wear tests indicated that the wear of the brush materials was intimately related to the voltage drop at the interface through a temperature-resistivity relationship. Materials having a high resistivity to conductivity ratio experienced high interface temperatures and wear. The heat which developed at the interface was caused by Joule heating due to current passage through the constriction resistance just inside the brush surface. For a given current level the voltage drop due to this constriction resistance was larger in materials with high electrical resistivity. Because Joule heating is the product of the constriction resistance and the current squared, brush materials having high electrical resistivity will dissipate large amounts of power in the contact region. Therefore, the relationship between the power dissipation at the contact and the wear rate was examined.

The Effects of Power Dissipated on Wear

Figure 12 shows the relationship between the power dissipated at the contact and the log of the wear coefficient. The power was determined from measured values of the voltage drop and current at each test condition. For each brush material, the wear coefficient increased exponetially with power dissipated in the brush. Because the wear results produced straight lines in Figure 24, the wear coefficient (C_w) could be modeled as:

$$C_w = A \text{ Exp } [B \cdot P] \qquad (10)$$

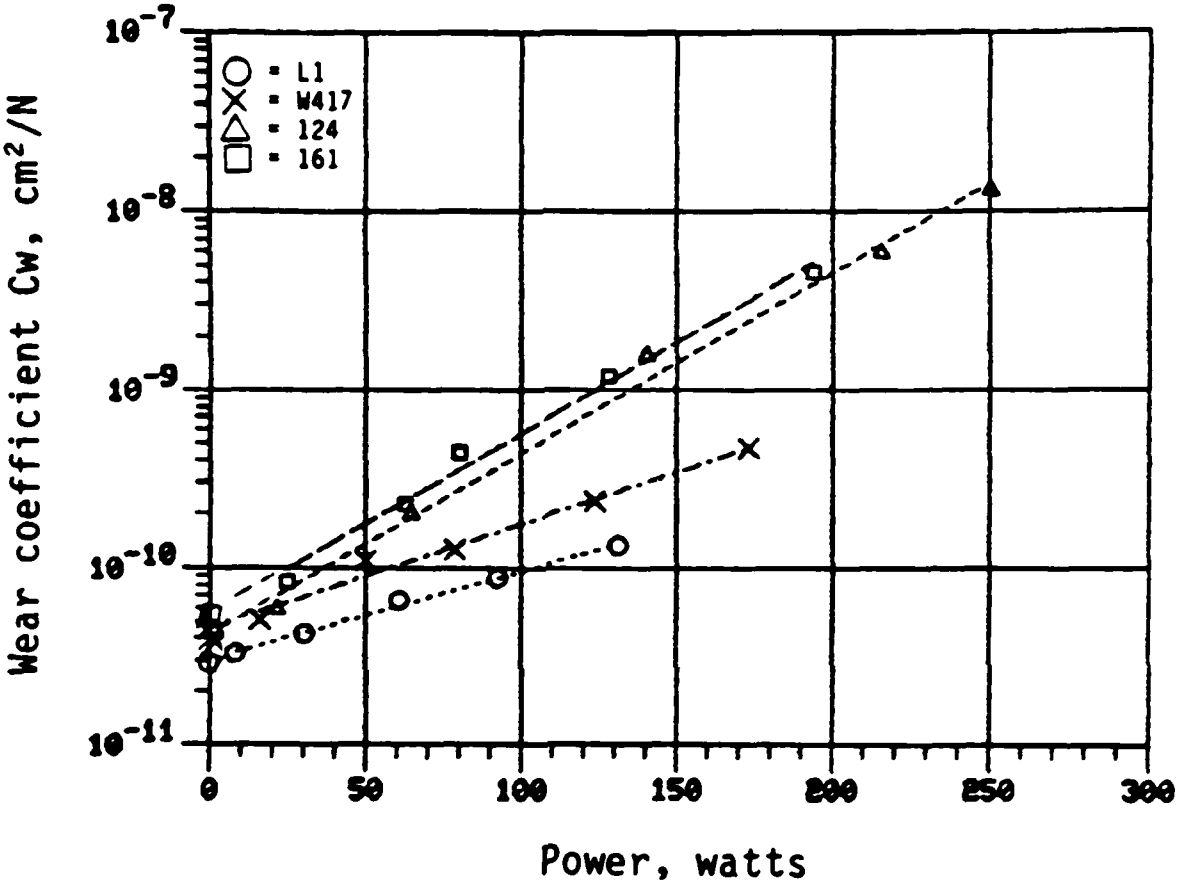

Figure 24. The variation in the wear coefficient with the dissipated power, 4.5 N load, 1620 rpm.

where

A and B = material coefficients to be determined

P = electrical power dissipated in contact

The statistical analysis of the data indicated that each material converged to the no-current wear coefficient at low power. With increasing power the wear coefficients diverged rapidly. The materials having a small r/k ratio displayed much smaller increases in wear with power than did materials having a high ratio. This ratio relates a material's ability to produce heat to its ability to remove heat. Materials with high ratios should thus experience higher contact temperatures at a given current level. As the operational parameters of load and speed were held constant for each of the materials tested, the factors leading to the divergence of the wear coefficients must be related to the thermal, electrical and mechanical properties of those materials.

Examination of the slopes found in Figure 24 indicated that the wear coefficient of a material increased proportionally to the ratio of resistivity to conductivity (r/k) to the 1/4 power. This relationship held for all of the wear test data. However, there was also a change in the wear coefficients with velocity and load. It was found that the semi-logarithmic slope increased proportionally to the sliding velocity and inversely to the applied load.

From this behavior a wear model could be formed which was dependent on the operational parameters of load and speed and the material properties of electrical resistivity and thermal conductivity. The general form of this model is:

$$C_w = C_w \text{ (no-current)} \; \text{Exp} \; [C_1 \; V \; / \; L \; (r/k)^{1/4} \; P] \qquad (11)$$

where

C_1 = constant
V = sliding speed (cm/sec)

The power is determined by multiplying the measured contact voltage drop by the measured current. This simple model fit the experimental data well, however, it still required the measurement of the voltage drop across the interface to determine the dissipated power. Ideally, a model could be developed where the material properties alone would be used in determining the voltage drop and thus the dissipated power and wear coefficient.

Constriction Resistance

The voltage drop is assumed to depend only on the constriction resistance and thus can be calculated for the contact. The constriction resistance was determined through a relationship developed by Johnson [10] for the operation of high current density electrical brushes. This expression was of the form:

$$Ro = 0.4 \; (r_c + r_{cu}) \; (\varepsilon H/nL) \; 0.5 + r_f \; (\varepsilon H/nL) \qquad (12)$$

where:

R_o = constriction resistance

r_c = electrical resistivity of the graphite

r_{cu} = electrical resistivity of the copper

r_f = surface film resistivity

ε = material hardness factor

H = material hardness

n = number of contact spots

L = contact load

The factor ε relates the contact hardness to the mode of deformation and has values of 1/3 and 1 for elastic and plastic deformation respectively. High temperatures at the contact ensure that all the deformation which occurs will be plastic, and the presence of a thermal mound on the contact surface reduces the number of contact spots to one. [11]. (The hypothesis of a single asperity is consistent to high speed pictures of the sparking phenomenon made by the authors.) Therefore, both ε and n are equal to one. The effects of the film resistivity and the resistivity of the copper may be ignored due to their small magnitude when compared to the other elements of this equation. Johnson assumed in the development of this expression that the contact spots are elliptical in shape and have a major to minor axis ratio of three. This leaves an expression of the form:

$$Ro = 0.4\ (r_c)\ (H/L)^{0.5} \qquad (13)$$

This expression is only dependent on the hardness and electrical resistivity of the brush material and on the load applied to the brush. The resistance of the brush can thus be easily determined.

Machine Dynamics

The load term used in equation (13) must be corrected for the effects of machine dynamics. The eccentricity of a rotor will produce a force which will tend to separate the brush/slip-ring contact. The load reduction resulting from such a force would tend to increase the constriction resistance and voltage drop. Shobert [4] has presented an equilibrium equation which allows computation of the speed at which an

equilibrium equation which allows computation of the speed at which an eccentric rotor will generate enough force to equal the load applied to the brush. This equation is of the form [4]:

$$\omega = 30/\pi \, [2 \, L \, / \, (M \, e)]^{0.5} \tag{14}$$

where

ω = rotational speed of the rotor in rpm

M = mass of the brush system

e = rotor eccentricity

Rearranging this expression and equating the separation force, F_S, produced by the rotor eccentricity with the load, L, applied to the brush, the load reduction may be determined for any rotational speed. This equation is of the form:

$$F_S = (\omega \, \pi/30)^2 \, (M \, e) \, / \, 2 \tag{15}$$

The remaining contact force (the difference between the force applied to the brush and the above separation force) is responsible for developing the contact patches. This remaining force, F', is easily determined by using the expression:

$$F' = L - F_S \tag{16}$$

The force F' must be used in equation (13) to compute the constriction resistance.

Values of F_S obtained from equation (15) were found to be much smaller than the load reduction forces determined from relative brush acceleration discussed in the dynamic tests. Equation (15) assumed a single wave per revolution but, measurements of the slip-ring indicated the presence of four high spots on its circumference. These additional

$$F_S = 5\ (\omega\ \pi/30)^2\ (M\ e)\ /\ 2 \qquad (17)$$

which was to be used with equations (5) and (8).

Using equations (13), (16) and (17), it is now possible to compute the constriction resistance of the contact when the material properties, load and speed are known.

Non-linear Voltage Drop

The temperature dependence of the electrical resistivity changes the value of the constriction resistance as the contact is heated. Therefore, the constriction resistance and voltage drop are current and temperature dependent. Bock [12] and Kaczmarek [13] carried out extensive work in the analysis of the current dependence of static, metallic electrical contacts. Their findings have shown that for such contacts there is a general relationship between the voltage drop and current of the form:

$$V_d = Ro + b\ (IRo)^m \qquad (18)$$

The values of the constants are related to a material's behavior while carrying current. Metals undergo conduction of heat and electricity largely through electron motion and will have large values of b and m. The behavior of a material with regard to its mode of conduction may be examined in part by the value of its Wiedemann-Franz-Lorenz constant. For purely electron conduction, as in metals, this constant has a value of $2.4\ (10^{-8})\ V^2\ {}^\circ K^{-2}$. For less conducting materials, the value of this constant increases. For typical graphites, the Lorenz constant is two orders of magnitude greater than for metals. The constants in the above voltage drop expression are inversely proportional to the Lorenz constant

and thus it would be expected that b and m would be lower for graphites than metals.

Based on data obtained during the wear tests, an analysis was conducted on the behavior of the voltage drop as a function of the current. A non-linear increase in the voltage drop was observed with current. From the data obtained in these tests the voltage drop-current relationship can be expressed as:

$$V_d = Ro + 0.75\ (IR_o)^{0.5} \tag{19}$$

Where Ro is determined by equations (13), (16), and (17).

Model Summary and Discussion

The wear model developed for the electrographitic brushes studied is dependent only on the machine dynamics and the material properties of the brush. For a known current level, it is possible to predict the wear rate of an electrographitic brush if the applied load, thermal conductivity, electrical resistivity, hardness, rotor eccentricity and sliding speed are known. This model will converge to the no-current wear coefficient for all electrographites studied and diverge rapidly with increasing current levels according to the material's ratio of r/k.

Combining the equations developed, the brush wear coefficient (C_w) may be expressed as follows:

$$C_w = C_{w_{(no\text{-}current)}}\ Exp\ [\ C_1\ V\ (r/k)^{1/4}\ V_d\ I\ /\ L\ ] \tag{20}$$

where $C_{w_{(no\text{-}current)}} = 3.0 \times 10^{-11}\ cm^2/N$ (for all brush materials studied)

V_d = contact voltage drop

$$C_1 = 2.72\ (10^{-2})\ \frac{g^4\ s^4}{cm^6\ C\ \Omega\ w^3}^{1/4}$$

and V_d due to the constriction is determined from the following expressions:

$$F_s = 5\ (\omega\ \pi/30)^2\ (M\ e)\ /\ 2$$

$$F' = L - F_s$$

$$Ro = 0.4\ r_c\ \ (H/F')^{0.5}$$

$$V_d = R_o + 0.75\ (IR_o)^{0.5}$$

Comparisions between the theoretical predictions of wear coefficient and the measured values are presented in Figures 25, 26, 27, and 28, for different operating conditions. These figures illustrate the behavior of the model as lines with symbols representing experimental points.

Figure 25 shows the theoretical and experimental values for the wear coefficient at 1620 rpm and 4.5 N load. The predicted wear coefficients were in agreement with the measured values with grade L1 showing the lowest wear and grade 161, the highest. The theoretical values predicted both the increase in wear with current and the slope of the wear curve for each of the brush materials studied. The model produced wear coefficients which were within a factor of 2 of the measured values over the entire range of current densities studied.

Figure 26 shows the predicted and measured wear at the higher sliding speed, but with the same load as Figure 25. The measured wear values are higher for this case where sparking was observed, but the model estimates these changes both qualitatively and quantitatively.

The effect of increasing the load is shown in Figures 27 and 28. Figure 27 is at the low speed condition where no sparking was observed.

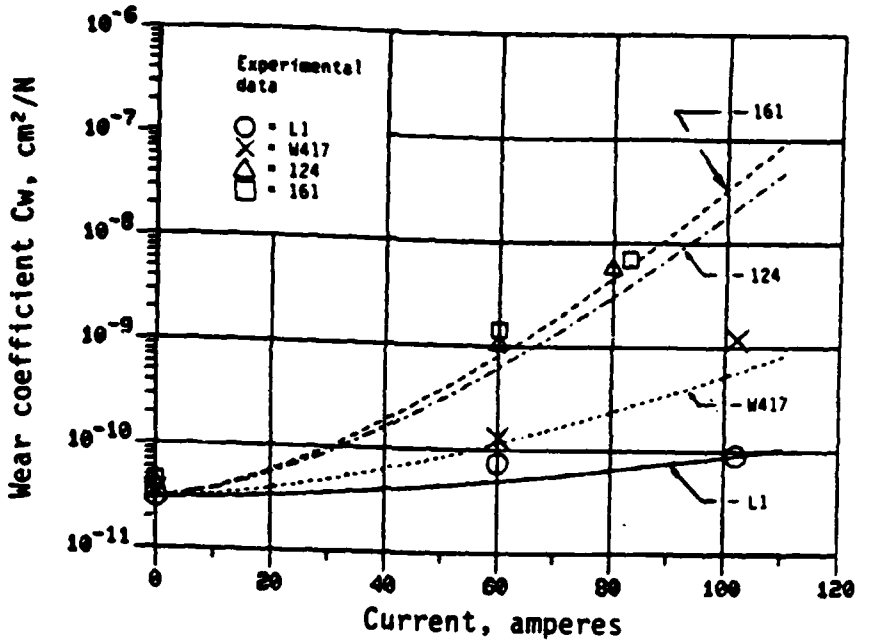

Figure 25. Theoretical model agreement with experimental data, 4.5 N load, 1620 rpm.

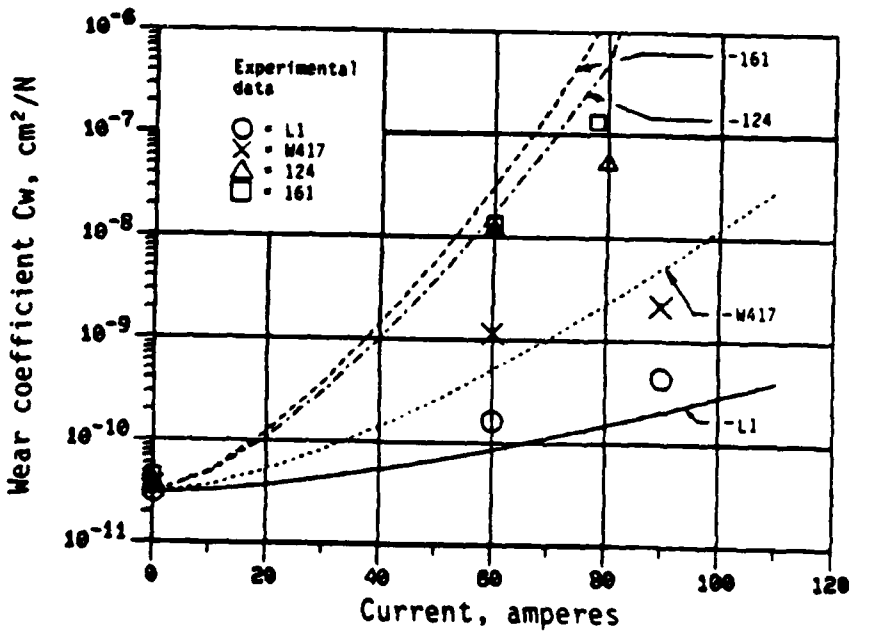

Figure 26. Theoretical model agreement with experimental data, 4.5 N load, 2750 rpm.

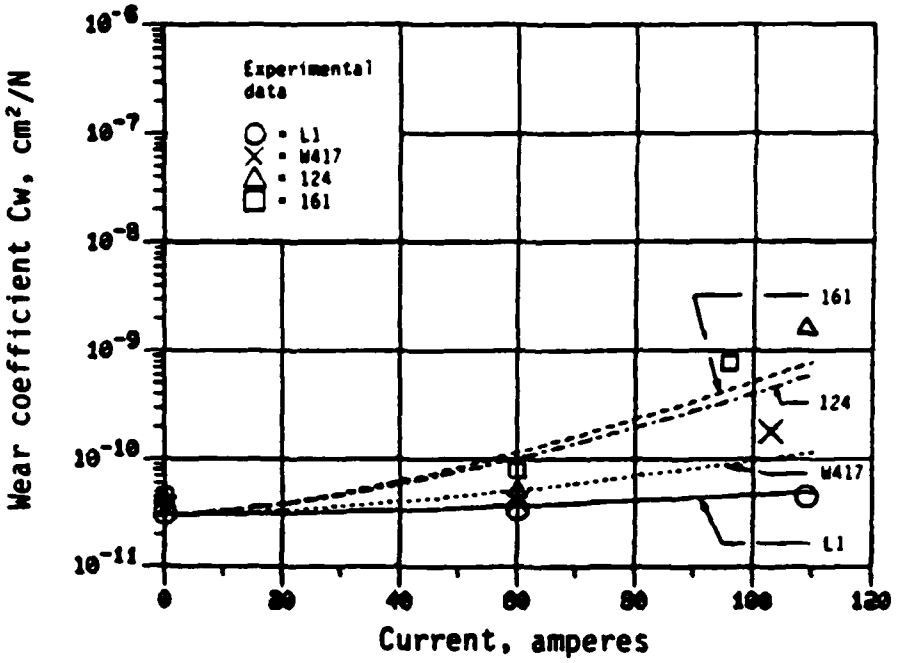

Figure 27. Theoretical model agreement with experimental data, 9 N load, 1620 rpm.

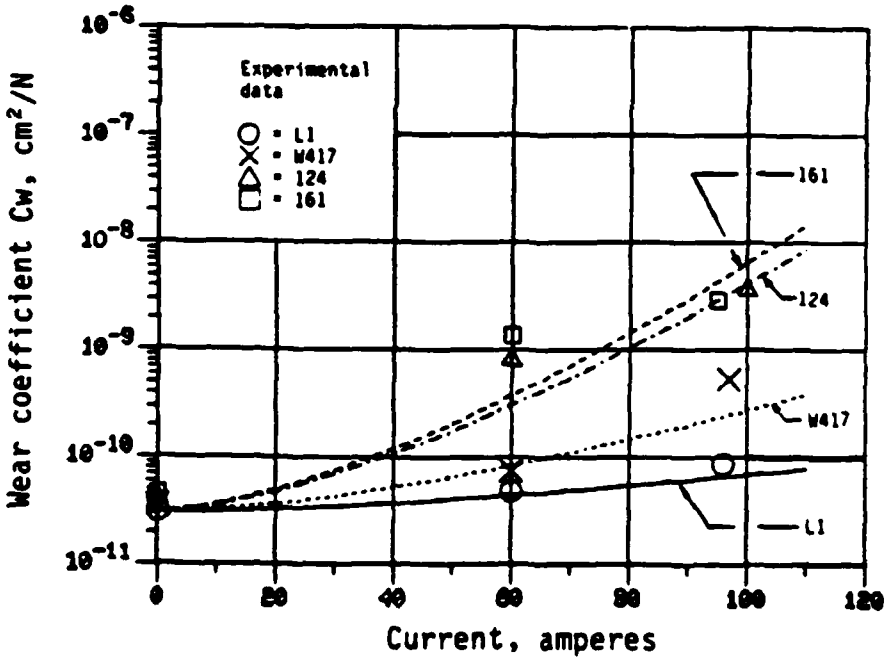

Figure 28. Theoretical model agreement with experimental data, 9 N load, 2750 rpm.

The predicted values of wear coefficient are within a factor of 5 for all the measured values. Figure 28 shows the wear at the high speed where sparking was observed. Again the model predicts the trends in wear measured. For all the operating conditions studied, the wear model predicted the measured values to within one order of magnitude. This is excellent agreement considering the broad range of materials and operating conditions examined.

The results of the wear tests and sparking tests have lead to the following senario for the wear of an electrographitic brush operating at high-current densities:

a) contact takes place in isolated spots based on the geometry of the brush and slip-ring.

b) current passage produces Joule heating to the constriction resistance in the vicinity of the contact spots.

c) The heating leads to increased local temperature and thermal expansion of the brush.

d) The brush distortion will lead to a single contact spot carrying both the mechanical and electrical load.

e) The dynamic effects introduced by slip-ring runout will reduce the brush load contact area and increase the constriction resistance and Joule heating.

f) When the local temperature exceeds a critical value (dependent upon the temperature-resistivity-conductivity behavior of the brush material) unstable heating at the junction occurs.

g) The resulting local temperatures are greater than 2000°C and, as a result, appear as visible hot spots at the interface.

h) A wear event occurs when these hot expanded region are removed from the brush by the sliding slip-ring. These hot particles leaving the surface are observed as "sparks."

i) Because the brush is hot and expanded in the vicinity of this wear event, the probability of subsequent contact in this region is increased. The behavior would lead to the observed traveling wave of hot spots on the brush surface.

Based on the agreement of the model with the experimental results, the above scenario represents a realistic hypothesis for high current density monolithic electrographitic brush wear.

REFERENCES

1. Dowson, D. History of Tribology, Longman, London, New York, 1979.
2. Martin, H. M. "Lubrication of Gear Teeth," Engineering, London, pp. 102, 199, 1916.
3. Grubin, A. N., and Vinogradova, I. E., Central Scientific Research Institute for Technology and Mechanical Engineering, Book No. 30, Moscow. (D.S.I.R. Translation No. 337) 1949.
4. Murch, L. E., and Wilson, W. R. D., "A Thermal Elastohydrodynamic Inlet Zone Analysis," Trans. ASME, Journal of American Society Lubricating Engineers, 1974.
5. Thermomechanical Effects Conference sponsored by ONR, June 19-20, 1979, Annapolis, Maryland, published in WEAR, Vol. 49, (1980); June 17-18, 1980, Columbus, Ohio, published WEAR, Vol. 79, (1982); June 18-19, 1984, Hanover, New Hampshire, to be published in WEAR in 1985.
6. Kannel, J. W., and Dow, T. A., "The Relation Between Pressure and Temperature in Rolling/Sliding EHD Contact," Trans. ASLE, Vol 23, 3, pp. 262-268, 1979.
7. Dow, T. A., "A Heat Balance in an EHD Contact," presented a the ASME Winter Annual Meeting, November 1980. (See also ONR Technical Report dated May 22, 1980).
8. Bowden, F. P. & Tabor, D., The Friction and Lubrication of Solids, Part II, pp. 104-105, Oxford: Clarendon Press, 1964.
9. Holm, R., Electrical Contacts Handbook, pp. 199-205, Berlin: Springer-Verlag, 1958.
10. Dow, T. A. & Kannel, J. W., "Thermomechanical Effects in High Current Density Electrical Slip-rings," WEAR, Vol. 79, pp. 93-105, New York: Elsevier/North Hollad Inc., 1982.

11. Shobert, E. I., Carbon Brushes, The Physics and Chemistry of Sliding Contacts, pp. 60-62, p. 77, pp. 150-152, New York: Chemical Publishing Co. Inc., 1965.

12. Williamson, J. B. P. & Allen, Nancy, "Thermal Stability in Graphite Contacts," WEAR, Vol. 78, pp. 39-48, New York: Elsevier/North-Holland Inc., 1982.

13. T. A. Dow and R. A. Burton, "The Role of Wear in the Initiation of Thermoelastic Instabilities in Rubbing Contact" Journal of Lubr. Tech. ASME, Vol 95, No 1.

14. T. A. Dow and R. D. Stockwell "Experimental Verification of Thermoelastic Instabilities in Sliding Contact" J. Lubr. Technol., Vol 99, No 3, 1977, p 359.

15. Roelands, C. H. A., Correlation Aspects of the Viscosity Temperature-Pressure Relationship of Lubricating Oils, O. P. Books Program, University Microfilm, Ann Arbor, MI, 1966.

16. Rabinowicz, E., Friction and Wear of Materials, p. 137, New York, John Wiley & Sons, Inc., 1976.

17. Jones, Llewellyn, The Physics of Electrical Contacts, pp. 157-158, Oxford: Oxford University Press, 1957.

18. Johnson, J. L. & Schreurs, J. "High Current Brushes VIII: Effect of Electrical Load," WEAR, Vol. 78, pp. 277, New York: Elsevier/ North-Holland Inc., 1982.

19. Marshall, R. A., "The Mechanism of Current Transfer in High Current Sliding Contacts," WEAR, Vol. 37, pp. 233-240, New York: Elsevier/ North-Holland Inc., 1976.

20. Bock, E. M. & Whitley, J. H. "Tunnel Film Resistance Utilizing Non-Linear Constriction Resistance Measurements," Proceedings of the Holm Seminar on Electrical Contact Phenomena, Vol. 16, pp. 45-50, 1973.

21. Kaczmarek, Jerzy & Kosmowski, Bogden B., "Constriction Resistance Measurements Based on the Method of the Third Harmonic," Proceedings of the Holm Seminar on Electrical Contact Phenomena, Vol. 19, pp. 155-157, 1973.

END

FILMED

3-85

DTIC